Molybdenum Thin Films:
Adhesion and Sodium Diffusion

by

Jeffrey Lee Alleman

ProQuest LLC.
789 East Eisenhower Parkway
P.O. Box 1346
Ann Arbor, MI 48106 – 1346

A thesis submitted to the Faculty and Board of Trustees of the Colorado School of Mines in partial fulfillment of the requirements for the degree of Master of Science (Materials Science).

Golden, Colorado
Date 6 April 1998

Signed: _____
Jeffrey Lee Alleman

Signed: _____
Dr. David LeRoy Olson
Thesis Advisor

Signed: _____
Dr. David Samuel Ginley
Co-Thesis Advisor

Golden, Colorado
Date 4/8/98

Signed: _____
Dr. John J. Moore
Professor and Chairman
Materials Science Program

ABSTRACT

Copper indium gallium diselenide (CIGS) thin film photovoltaic cells are typically deposited on molybdenum coated, soda lime glass substrate. The back contact of the device is a sputter deposited molybdenum layer. During deposition of the CIGS, thermal expansion mismatch at the CIGS/molybdenum/soda lime glass interfaces can create adhesion problems. Methods to improve adhesion especially to the glass substrate such as the deposition of a chromium interlayer, etching the glass surface and minimizing the residual stress of the deposited molybdenum through control of process parameters were investigated. The deposited molybdenum films were analyzed for thickness, sheet resistance and adhesion. The CIGS cells with a layer of chromium show a consistent small lowering of the open circuit voltage and efficiency. Sodium diffusion from the soda lime glass is beneficial for CIGS device performance. The affects of oxygen (as reflected in the O_2/Ar ratio during sputtering) were also examined over the range of 0-20 percent oxygen. The sodium diffusion was analyzed with SIMS depth profiling and X-ray diffraction was used to examine the molybdenum structure and residual stress. Essentially no change in sodium diffusion was observed over this range of oxygen partial pressures.

TABLE OF CONTENTS

LIST OF FIGURES

LIST OF TABLES

ACKNOWLEDGMENTS

I want to express my gratitude to my thesis advisor, Dr. Dave Olson and co-advisor, Dr. Dave Ginley, for their guidance on this project. I would also like to thank Drs. John Moore and John Trefny for serving on my committee. The Materials Science department who took a chance on a part-time student with a less than stellar academic record.

The work reported on in this thesis was completed at the National Renewable Energy Laboratory (NREL) and I would like to thank my co-workers that helped. Dr. Rommel Noufi for suggesting the work to be done, for useful discussions and for serving as a committee member. Dr. Falah Hasoon and James Keane for the fabrication of CIGS cells Dr. Sally Asher for SIMS analysis and helpful discussions on interpretations, and Jennifer Granada for useful discussions on the effects of sodium diffusion.

Finally I would like to thank Teresa, my friend and future wife for understanding and support during all the late nights and early mornings that went into the preparation of this thesis.

1. INTRODUCTION

Copper indium gallium diselenide (CIGS) thin film photovoltaic cells are solid state devices that convert sun light to electrical energy. One measure of a photovoltaic cell is based on the conversion efficiency for sunlight to electricity. The best CIGS cell to date has an efficiency of 17.7 percent[1]. Cell efficiency can be affected by all the steps during the fabrication process. Substrate selection can affect all subsequent processing steps and ultimate conversion efficiency. Substrates which have been used to make successful devices are soda lime glass, borosilicate glass, stainless steel, alumina, and high temperature polyimide[2,3]. The highest conversion efficiency devices are on a soda lime glass substrates. The beneficial diffusion of sodium from the soda lime glass has been credited with improving the efficiency[4,5]. The soda lime glass and the molybdenum back contact was examined. The morphology of the sputtered molybdenum film and degree of oxygen contamination effects how the sodium diffuses.

1.1 CIGS Thin Film Photovoltaics

A cross sectional view of a typical copper indium gallium diselenide photovoltaic is shown in Figure 1-1. The basic process as employed at National Renewable Energy Laboratory is described. The back contact is a sputtered layer of molybdenum 1 μm thick.

The use of molybdenum as a back contact started because of the need for an ohmic contact that could resist the effects of selenium, be easily deposited and be cheaper than gold [6,7].

The CIGS absorber layer (p-type) can be deposited by several methods[8,9]. In the laboratory, thermal co-evaporation has demonstrated the highest efficiency[1]. Thermal co-evaporation allows for exact control over the rate of deposition of the individual elements allowing accurate compositional control during the formation of the absorber layer.

Another approach deposits multiple layers of copper and indium by sputtering; then selenium is evaporated in the last step. Sputter deposition has employed compound targets. Difficulties have been encountered with this approach because of preferential sputtering of the elements[10].

Chemical bath deposition is used to deposit a 50 nm layer of cadmium sulfide on the absorber layer[11,12]. The n-type cadmium sulfide forms a hetrojunction with the p-type copper indium gallium diselenide. Recent work however has shown that the semiconductor junction is in the top of the absorber layer[13].

The zinc oxide window layer is deposited by sputtering using an RF magnetron. The intrinsic layer is sputtered in an argon-oxygen atmosphere to maintain stoichiometry. The second layer is the n-type doped ZnO/Al sputtered in argon only. The top contact of the cell is finished by a nickel aluminum metal grid deposited onto the zinc oxide layer to minimize electrical losses due to the high sheet resistance of the zinc oxide.

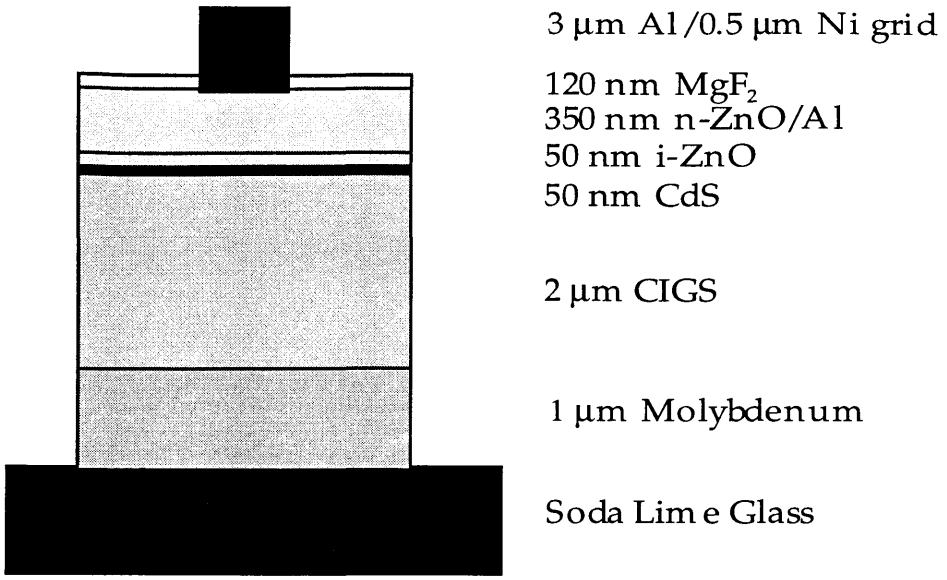

Figure 1-1. Cross section of a copper indium gallium diselenide photovoltaic device.

Cells can then be finished with deposition of an antireflection layer of magnesium fluoride[14]. Through all the steps fabrication of a copper indium gallium diselenide cell requires four vacuum deposition systems and one chemical bath deposition step.

1.1.1 The Soda Lime Glass Substrate

Soda lime glass is an ideal choice for the substrate because of the low cost in comparison to other substrates. However the soda lime glass contains many alkali metals that can diffuse out during the high deposition temperatures required for the absorber layer

and become impurities in the absorber. Sodium, however, appears to be beneficial. Recent studies have shown sodium that has diffused from the soda lime glass beneficially affects the copper indium gallium diselenide cells efficiency[5]. Sodium has shown to be important in the formation of large grains in the absorber layer[15]. An understanding of the sodium diffusion through the molybdenum and into the copper indium gallium diselenide layer appears to be necessary to make the highest efficiency devices.

Repeatability in the deposition of the absorber layer depends on control of all the process variables. After the absorber layer has been deposited the surface has sodium present. The amount of sodium on the surface varies depends in a large part on the rate of diffusion of the sodium through the molybdenum film in a localized area. The molybdenum layer then must be examined to understand the diffusion of sodium from the soda lime glass.

1.1.2 The Molybdenum Back Contact

The cross section morphology of sputtered molybdenum thin films looks like a cross section of shag carpet with columns of molybdenum grains packed together to form the molybdenum layer Figure 1-2. The columnar grains exhibit a localized crystalline grain structure. Literature has described for sputter deposited metallic films under similar conditions of the molybdenum deposition to have defects such as vacancies, dislocations and dangling bonds making impurity formation simple. Impurities such as oxygen come from residual gasses and water trapped in the surface of the vacuum chamber. Every time the chamber is exposed to atmospheric conditions the walls adsorb contaminants.

Secondary Ion Mass Spectrometry (SIMS) has shown the oxygen content to change under different sputter conditions[16].

The sputter deposition method also incorporates stress into the film[17,18]. The intrinsic stress of the molybdenum film can be compressive or tensile in nature, depending on deposition conditions of argon pressure and sputter power[19]. The amount of energy of the sputtered particle is controlled by the pressure and mean free path between collisions of the atoms in the plasma and the voltage potential. The bombardment of the molybdenum film by the energetic particles determines the stress[20]. The nature of intrinsic stress of a film is covered in the sputtering section.

The sputtered molybdenum has also produced adhesion problems in the way of buckling of the CIGS/molybdenum layers and subsequent peeling after the absorber layer growth. The bonding of the molybdenum film to the soda lime glass can have several types of bonds[21]. When the energitics of the deposition are low that the deposited adatom has no surface mobility on the substrate surface and does not interact with the surface. An abrupt transition from the soda lime glass surface to molybdenum layer forms in the distance of a monolayer. Little chemical interaction happens between the two different layers. A weak bond of the molybdenum to the soda lime glass results.

The next type of interface is a chemical bonding interfacial layer where chemical reactions with the substrate occur over several atomic distances. The chemical reaction occurs with the molybdenum atoms and the soda lime glass and may be affected by residual gases.

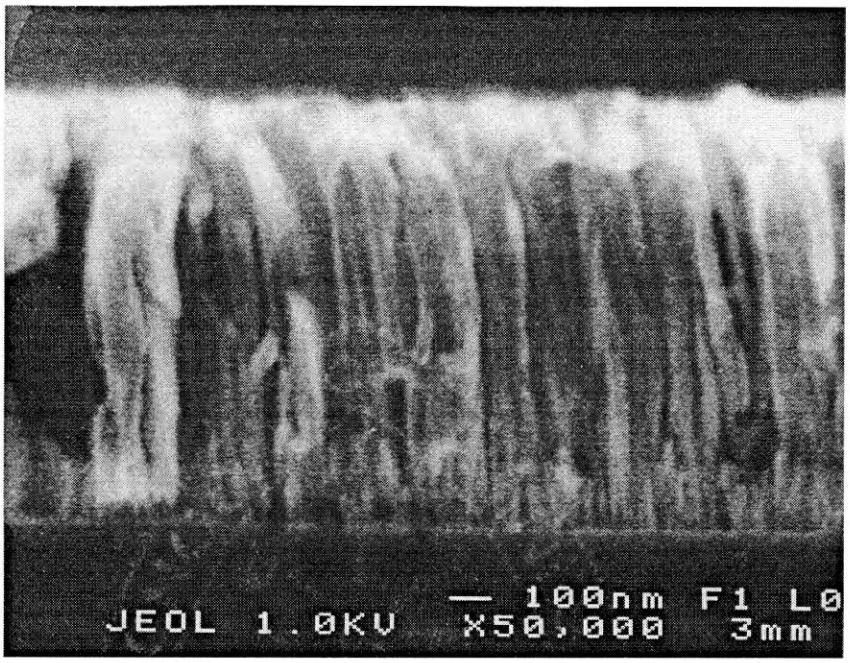

Figure 1-2. A micrograph of a 1.2 μm sputtered molybdenum thin film on soda lime glass. The conditions for growth were 2 mTorr of argon and a substrate temperature of initially 20° climbing to 120° Celsius during deposition.

The last is a pseudodiffused interfacial layer resulting from an implantation process of high energy molybdenum atoms from the sputtering plasma and back sputtered soda lime glass particles which mix and condense on the substrate surface. The molybdenum atoms have sufficient energy to penetrate the substrate surface a few atomic layers when the sputter pressure is low where the mean free path for gas collisions is greater than the target to substrate distance. The energetic plasma conditions will sputter atoms from the substrate with the high energy argon atoms. The two effects of the plasma work together to increase the strength of the molybdenum bond.

When the substrate and molybdenum film are heated during the CIGS deposition a thermal expansion mismatch between the molybdenum and soda lime glass can cause cracking of the molybdenum film. Table 1-1 shows the coefficients of thermal expansion for the three materials. The soda lime glass thermal expansion coefficient is approximately two times larger then that for molybdenum. The softening point of the soda lime glass is at 550° C. The expansion of the glass at the softening point is such that cracks in the molybdenum result from the tensile loading caused by the greater expanding soda lime glass. The CIGS deposition process has better grain formation at higher temperatures. The temperature for the CIGS deposition is then right at the softening point of the soda lime glass. Crack formation can come about from a rapid cooling rate where the soda lime contracts and the compressive stress is sufficient to buckle the molybdenum film. The severity of the buckling depending on the adhesion of the molybdenum to the soda lime glass substrate.

Table 1-1. Room Temperature Thermal Expansion Coefficients.

Material	Thermal Expansion Coefficient $\alpha(x10^{-6}m/°C)$
Soda Lime Glass	9.2
Molybdenum	5.1
Copper Indium Diselenide	8.2

1.2 Physical Vapor Deposition

Vapor phase deposition of an element is typically accomplished under vacuum where contamination from the environment is minimized. However many deposition processes require a minimum of several mTorr of vacuum pressure to work. To deposit a molybdenum back contact two methods of deposition are employed. The first method is the electron beam evaporation of a thin chromium adhesion layer. The second method is sputtering with a DC magnetron, used for the molybdenum layer.

1.2.1 Sputtering

Sputtering[17] was first used as early as 1877 for coating thin metal films on glass for mirrors. In 1930's Western Electric sputtered gold films down as conductors prior to subsequent electrodeposition of gold. Because of the slow rates of deposition associated with sputtering, thermal evaporation and electron beam evaporation became the preferred methods. Interest in sputtering did not increase until the 1960-1970's when magnetic confinement fields were introduced to increase the sputter rate and thereby making sputtering a practical industrial process[22].

Typically the vacuum chamber used for sputtering is evacuated then an inert gas, like argon, is introduced into the chamber and the pressure is maintained at a few mTorr. The flow rate of the gas is dependent on the vacuum chamber geometry and pumping system capacity. Composite targets can be sputtered that would decompose in thermal evaporation. Sputtering in a reactive ambient can produce composite films such as ZnO

from zinc target and oxygen. Other attributes of sputtering are the ability to coat large areas with uniform thickness, the ability to control deposition rates run to run, and the ability to use conducting and nonconducting targets. Semiconductor devices not sensitive to damage from a high energy particles can be processed this way.

The direct current (DC) magnetron is used to sputter conducting targets. A strong magnetic field is used to concentrate the secondary electrons of the ionization and sputtering process back into the plasma ionizing the argon further. Any fast moving electrons that the magnetic field can not contain are repelled by the negative voltage of the cathode but not in a focused direction. Different configurations of the magnetic field allow the target to be cylindrical (hollow or post), planar or ring. The target shape used for various coating processes is dependent upon the shape of the substrate and the throughput desired. For the molybdenum sputtering done in this study a DC planar magnetron is used as shown in Figure 1-3.

The magnetic confinement allows for sputtering pressures of less than 1 mTorr up to 100 mTorr and lowers the applied DC voltage needed to maintain a plasma. The rate of sputtering can be described by the sputtering yield, S, of the number of sputtered molybdenum atoms to incident argon ions is 0.9 for a 600 Volt power source. The ratio of S can be found kinetically by determining the nuclear stopping power, s(E),involving the energy transfer function where E is the electric field, and m_i and m_t represents the mass of the sputter ion and the target ion[23].

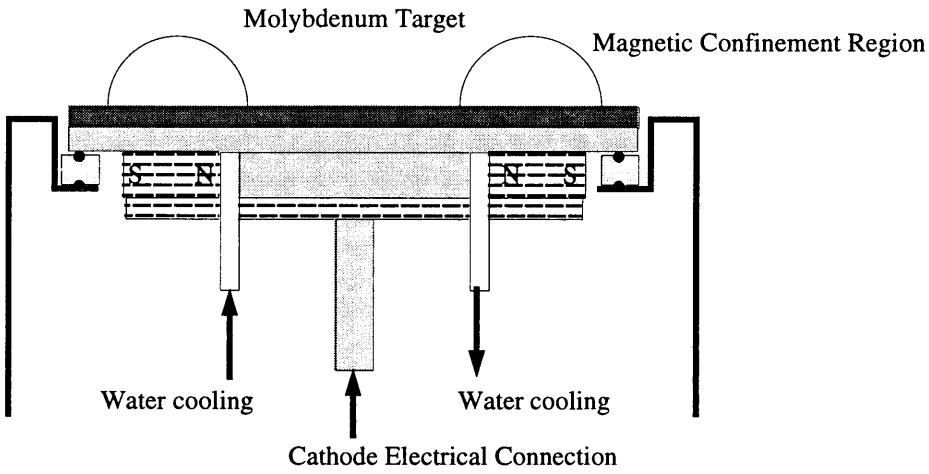

Figure 1-3. Cross section of a planar DC Magnetron Cathode.

$$s(E) = \frac{m_i m_t}{(m_i + m_t)^2} E * \text{constant} \quad (1)$$

The sputtering yield is then calculated from the following equation:

$$S = \frac{3\alpha}{4\pi^2} \frac{4 m_i m_t}{(m_i + m_t)^2} \frac{E}{U_0} \quad (2)$$

where U_0 is the binding energy of the surface and α is the ratio of the target atomic mass to the sputter gas atomic mass m_t/m_i. The sputtered molybdenum atom has kinetic energy of less than 1 eV. The E_k less than 1 eV is a best estimate from data on other metals. The sputter power density affects the growth of the film and the magnitude of intrinsic stress in the deposited molybdenum layer. DC planar magnetron sputtering is used extensively for physical vapor deposition of thin films in industries from microelectronics to decorative coatings. The thin films produced are normally conducting metal films where sputter deposition is the simplest method. Many factors influence thin film growth during deposition with substrate temperature and bias voltage as the dominant controlling factors. Simple nucleation and growth models do not adequately account for observed thin film growth due to the low energy of the depositing atoms[24]. The empirical structure zone model describes the observed film growth characteristics based on a ratio of substrate temperature to melting temperature of the material to be deposited.

1.2.2 Electron Beam Evaporation

The chromium adhesion layer used in the study was deposited by electron beam evaporation. Electron beam evaporation consists of accelerating an electron beam into the surface of the material to be heated to the point of evaporation. The electron beam is generated through thermionic emission from the cathode filament. Using currents of a few milliamperes to amperes and an accelerating voltage of ten thousand to thirty thousand volts heating energies of two hundred kilowatts can be obtained. The heating by the bombardment of the electrons is sufficient to evaporate any element. In addition many compound materials can be deposited by this method. The chamber pressure must be below a pressure of 10^{-4} Torr to limit collisions with the gaseous atoms preventing scattering of the evaporated atoms. The high voltages can be maintained in this vacuum without arc discharges occurring. The small laboratory electron beam systems use a transverse cathode for systems of up to 200 kilowatts of power and larger systems use a direct electron beam. Figure 1-4 shows a cross section of an electron beam source. The beam is electromagnetically steered over the source pocket. The electron beam is continuously swept across the molten surface of the material to be evaporated. The hearth is water cooled to prevent reacting with the melt.

Contamination from residual gases from the vacuum system is minimized but as a general rule for depositions in the 10^{-6} Torr pressure range a monolayer of condensing atoms strikes the surface of the substrate every second. The better the vacuum the less contamination during deposition.

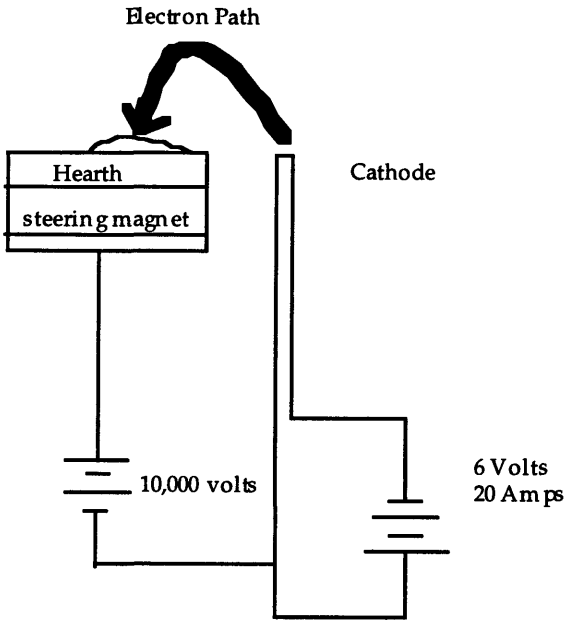

Figure 1-4. Schematic of electron beam deposition system.

1.3 Growth Models

Thin film growth has been classified into several stages[25]. The first stage is film nucleation where deposited atoms begin to coalesce into clusters around nucleation sites[26]. The clusters grow to impingement and start the growth of columns. The thin film growth is affected by the temperature of the substrate and the rate of deposition[27]. The resulting structure in the film can be highly stressed[20,28,29]. The Thornton model and recent work with computer simulations are briefly illustrated for growth of a sputtered thin film.

1.3.1 Structure Zone Model

The nucleation and growth of vapor deposited thin films follows the structure zone model for grain growth as shown in Figure 1-5. The model was developed by Movchan and Demchishin[30] and later refined by Thornton[31]. The model is based on emperical observation. Four types of growth regions based on substrate temperature, sputter pressure, and the ratio of substrate temperature to melting temperature of the deposited material are depicted.

The structure zone model is based on physically observed growth at varied process conditions for sputtered materials. Zone 1 (T_S/T_m <0.1)[27,31] is characterized by dome topped columnar growth of small grains. Crystalline and amorphous deposits can form in this zone. The columnar grain will extend the thickness of the film with the internal structure poorly defined with many defects. The column diameter increases with the ratio T_S/T_m, does indicating low surface mobility of the adatom. Metallic films are hard but have

no lateral strength. The low mobility leads to shadowing of the growing crystals peaks. Open boundaries are formed in the film, especially for deposition at an oblique angle. The surface roughness forms from the initial shape of the nuclei or preferential nucleation on the substrate and preferential growth. Elevated gas pressure results in intergrain boundaries becoming more open and increase in residual gas entrapment. The crystals tend to point in the direction of the coating flux vector. The change comes about from reduction of the mean free path and lowered adatom mobility.

Zone T ($0.1< T_S/T_m < 0.3$), is the transition zone proposed by Thornton, here the adatoms have partial mobility and surface diffusion can take place. The effects of shadowing and voids are thereby less pronounced. The grain boundaries are dense and the mechanical strength is improved. The columnar grain structure has local epitaxy within each grain that is repeated in the next grain. The surface roughness and initial nucleation can be overcome to form a smooth surface. Thin films with bcc, fcc and hcp structures have been observed to form with their most densely populated face one the substrate.

Zone 2 ($0.3 < T_s/T_m < 0.5$), columnar grains continue to grow with the diameter less than the thickness of the film. Surface diffusion and grain boundary migration occur to form dense intercrystalline boundaries. At higher T_S/T_m ratios, the grains will extend the thickness of the film.

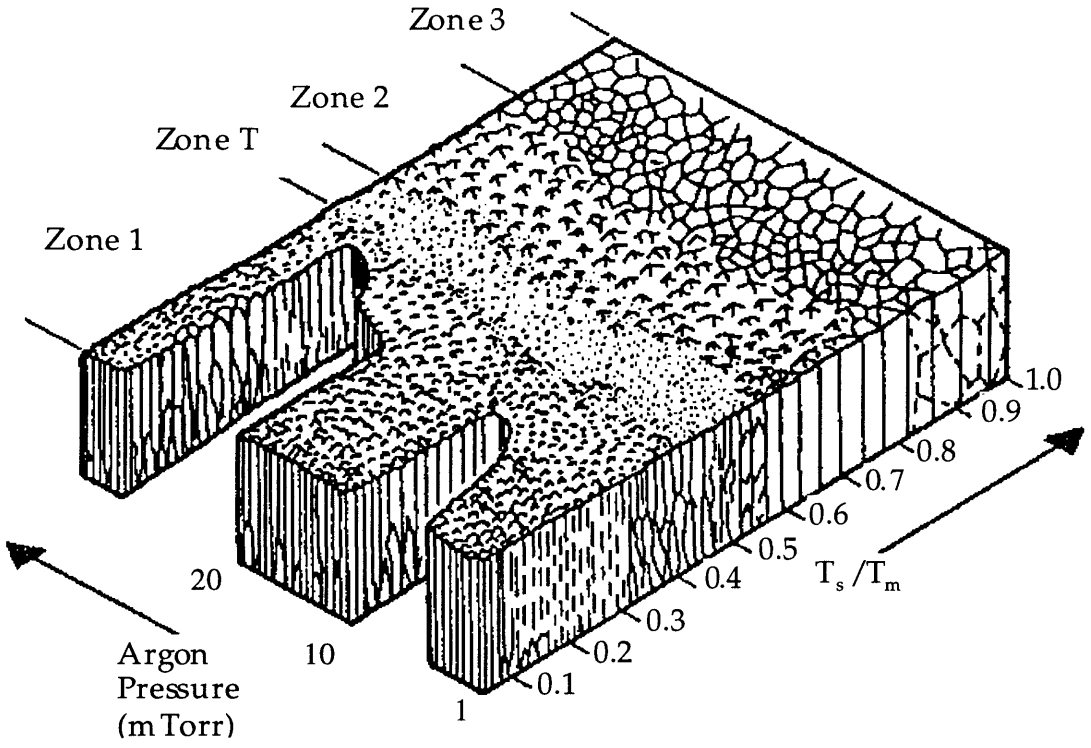

Figure 1-5. The Thornton diagram showing the relation of observed film growth for conditions of sputter pressure as a function of the ratio of substrate temperature to the deposited material melting point.[31]

Zone 3 ($0.5 < T_s/T_m < 1$), bulk diffusion has a dominant effect on the final structure of the film. Grain growth is promoted such that grains can be several times larger than the thickness of the film. For a metal the properties and structure correspond to a fully annealed metal. Variation in the grain size maybe a result of bulk diffusion or recrystallization.

In our case for the molybdenum with a melting point of 2616° C and a substrate temperature of 120° C the T_s/T_m ratio is 0.046 suggesting growth in the Zone 1 region for all sputter pressures. During sputtering the substrate experiences fluxes of different particles besides the sputtered molybdenum atoms[23]. Figure 1-6 illustrates the flow of the energetic particles. Reflected neutral atoms include argon atoms and impurities like oxygen. The fast neutral atoms are generated by picking up kinetic energy from collisions with sputtered molybdenum atoms and have sufficient energy to back sputter atoms from the substrate. The energetic particles do influence the film growth. The growth can be shifted into the zone T region where localized ordering will take place.

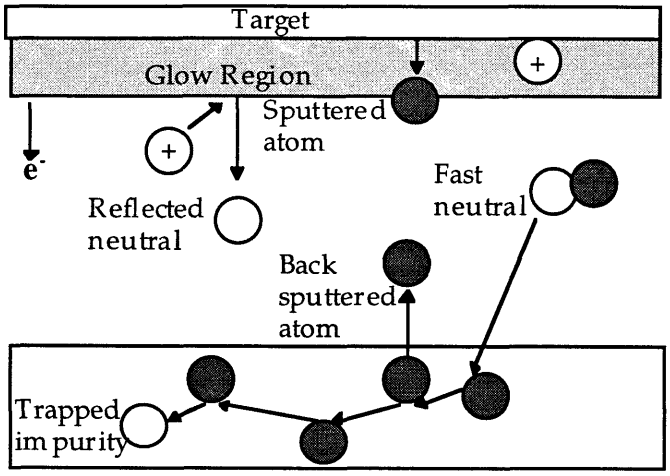

Figure 1-6. Different species that the substrate surface is exposed to during growth.

1.3.2 Ballistic Growth

The Ballistic Growth model[32,33] describes two dimensional growth explaining channel and void formation (Figure 1-7). An assumption of this growth model is that the adatom sticks where it hits. Surface and grain boundary diffusion are considered insignificant. Voids are formed when a position is not filled leading to a shadowing effect as higher neighboring columns block the pathway of subsequent incident atoms. The columnar growth is inclined at an angle β to the surface normal. Other simulation work[34,35] has reported that the angle follows the tangent law $2\tan\beta = \tan\alpha$ where α is the particle incidence angle relative to the substrate surface normal. In the simulation shown in Figure 1-7 the incidence of particles is at forty five degrees, β is measured at eighteen degrees (represented as the dashed line) and the tangent law predicts twenty six degrees (shown by the solid line). Further evaluation showed that the ratio of the probability of the adatom to stick in a windward or leeward site of a column and the resulting horizontal displacement at the site lead to $\tan\beta = (p/q)/\sqrt{3}$ which adequately describes β[32]. The simulations are in a two dimensional world and in reality the adatoms have three dimensions. In the case of sputtered films the angle β closely follows the tangent law. The theory is not settled on the mechanisms that control the angle β as yet.. The voids form a network of void columns that are much smaller in size to the columns. Impurities are trapped in the voids formed.

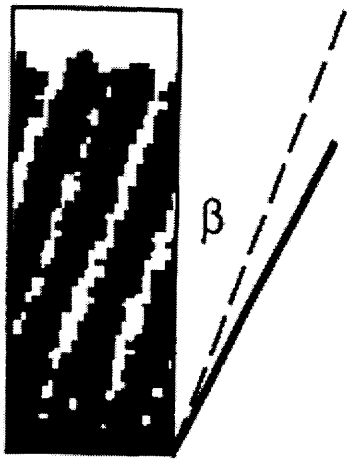

Figure 1-7. Ballistic growth model[32] demonstrating void column formation in relation to flux incidence angle β.

1.4 Grain Boundary Diffusion

In multilayered thin film structures, such as microelectronic devices interdiffusion is commonly seen at temperatures lower than in the bulk form[36]. The kinetics for thin films with small grain size, and the presence of grain boundaries with impurity defects and clean interfaces can produce diffusion rates several orders of magnitude greater than bulk diffusion rates[37]. The grain size decreases with increasing elemental melting temperature and substrate temperature. For the molybdenum thin films with a columnar grain diameter of 100 nm, about half an atomic percent of the atoms are located on the grain boundary[38]. The larger concentration grain boundaries will allow for fast grain boundary diffusion of sodium in the case of the CIGS device.

In the best circumstances thin films made through the sputtering and evaporation process are polycrystalline. Thin film diffusion was discussed as early as 1935[39,40]. Typically the thin film structure is filled with defects along the grain boundaries making diffusion at room temperature possible. The integrated circuit industry has known for many years that diffusion along the grain boundaries for immiscible elements is possible[41]. The rule of thumb for diffusion in a material is when the temperature is above 0.5 T_m to 0.66 T_m bulk diffusion dominates; below 0.5 T_m grain boundary is diffusion controlled.

Control of diffusion has been accomplished by adding barriers that act to block the atomic transport. The diffusion barrier location depends on the application such as at the substrate or the surface of each grain of the film. There are several barrier types consisting of thermodynamically stable, semi-stable, sacrificial and stuffed barriers[41]. The barrier layers are derived from metallization schemes for integrated circuits where an undesirable metallic species is prevented from diffusing into the device and destroying the semiconductor junction.

A thermodynamically stable barrier is a compound with a large negative free energy of formation that separates two layers. Further compound formation on each side of the separation film would not be possible because of the positive free energy of such a reaction relative to the formation of the barrier compound. The interface becomes an area where diffusion of a barrier element out of this film is thermodynamically uphill. Chemical compounds of oxides, nitrides, borides, silisides and carbides are strongly bonded compounds.

A partially stable thermodynamic barrier is a layer with a lower free energy with respect to a reaction with either layer being separated. The barrier layer will not guarantee a low diffusion between layers only that the barrier X will not react. An example of a partially stable barrier is on a silicon wafer with a gold contact. A lead solder contact to the gold layer would have an undesirable reaction. To prevent mixing of the gold and lead an alloy of silver and gold was found. The alloy bound up the gold chemically with a lower free energy in relation to a reaction with the lead [42,43].

A sacrificial barrier layer is put between two layers to separate them during a high temperature processing step. The thin film reactions with the layers must be laterally uniform and the activation energy and rate of reaction known. The sacrificial layer thickness is determined such that a partial thickness is left after the high temperature process step. The time before intermixing will occur can be measured and then used in a predictive fashion to establish necessary barrier thickness.

A stuffed barrier has potentially easy diffusion paths along the layer grain boundaries plugged by impurities. The stuffed barrier was observed in some metallization schemes where an element was thought to provide a diffusion barrier when in fact the grain boundaries of the layer were plugged with impurities of oxygen and nitrogen from the deposition system. An example of this situation is the titanium/molybdenum/gold metallization[44]. Molybdenum and gold do not normally intermix but gold diffusion is possible along the grain boundaries of the molybdenum. At six hundred Celsius intermixing of the titanium and gold occurs. The intermixing is prevented by the application of oxygen to the titanium layer before the molybdenum deposition. The formation of a thin titanium dioxide layer prevents intermixing of the titanium,

molybdenum and gold. The success in this metallization scheme is derived fortuitously because of poor vacuum conditions during the deposition of the titanium layer. The distinction between a stuffed barrier and a thermodynamically stable compound layer is not always clear.

1.5 Sodium Effects On CIGS Grain Size And Device Efficiency

In a study on the sodium concentration needed for increased device performance, Granata[4] saw beneficial effects for concentrations between 0.05-0.5 atomic percent. An increase in the open circuit voltage V_{OC} and device fill factor was observed. Capacitance measurements showed an increased hole density with increasing sodium concentration. At 1 atomic percent sodium the hole density concentration had increased three orders of magnitude over lower sodium concentrations of 0.05-0.5 atomic percent and the device started to degrade because of possible secondary phase formation. Suggested electronic models for the role of sodium in CIGS devices can be found in the literature of Zhang[45] and Neumann[46].

Sodium acts as a fluxing agent during growth, the grain size is increased, defects are reduced and an increase in orientation of the CIGS grains thus giving better device performance. The enhanced grain growth could be due to the existence of a compositional gradient of the sodium. In the enhanced grain growth model of Olson and Edwards[47] the forces of surface tension are equated in Figure 1-8. If a compositional gradient is added such that the grain boundary tension is lowered the grains would be able to grow further.

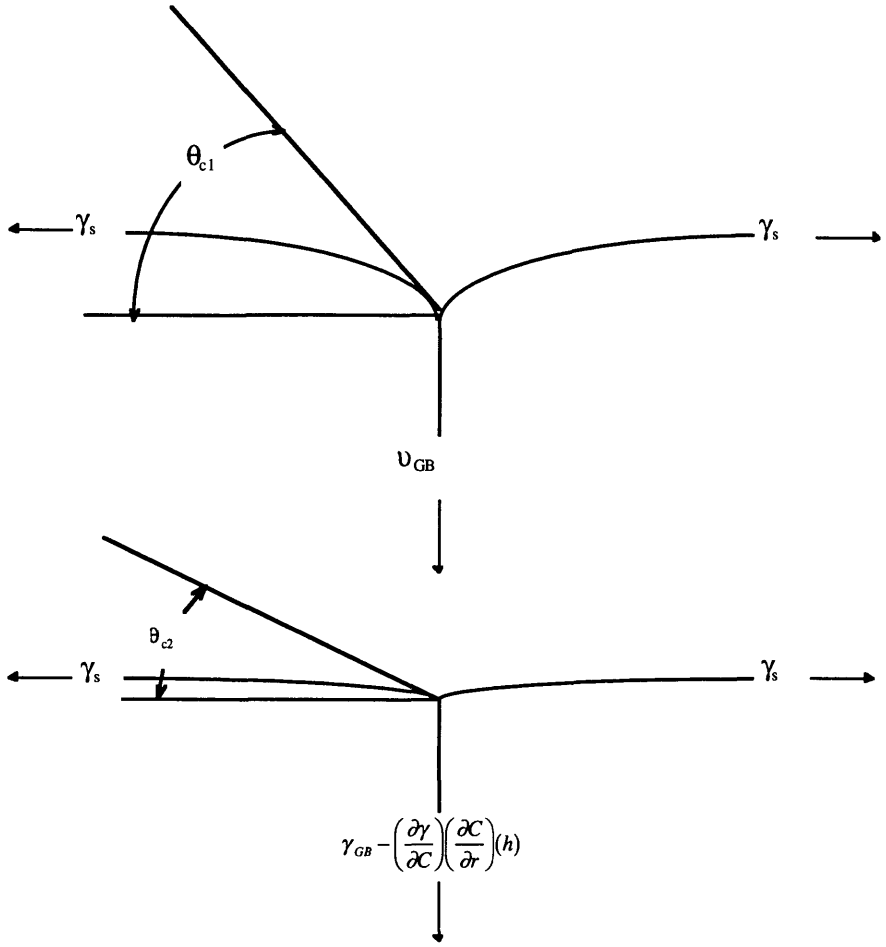

Figure 1-8. Grain boundary cross section with surface tension forces.

After nucleation and grain impingement the grains are forced to grow vertically and the grain boundaries can serve as pinning sites which would stagnate further growth. In the normal grain growth model of Mullins[48] the triple points where the grain boundary meets the free surfaces is where the growth stagnates. Surface diffusion redistributes the matter at the triple point to balance the interfacial tensions. The boundary of the two grains forms a groove at the surface. The angle θ_0 is determined by the force balance of the interfacial tensions. The angle can be used to measure the force by which the grain will need to pull out of the grove and continue growth. A driving force needs sufficient strength to overcome the critical angle $\theta_{critical}$ for the grain boundary to climb out of the grove as described by:

$$\theta_c = h\frac{k_{critical}}{2} \tag{3}$$

where h is the film thickness, γ_S is the surface tension, γ_{GB} is the grain boundary tension and the critical curvature for escape is $k_{critical}$ which is described by:

$$k_{critical} = \frac{2\theta_c}{h} = \frac{\gamma_{GB}}{\gamma_s h} \tag{4}$$

Now with a solute or contaminant compositional gradient $\partial C/\partial X$ at the grain boundary, such as the sodium compositional gradient, the force balance is altered. An additional term is suggested in the following:

$$2\gamma_s \cos\theta_c = \gamma_{GB} - \left(\frac{\partial\gamma}{\partial C}\right)\left(\frac{\partial C}{\partial r}\right)h \tag{5}$$

If the grain boundary tension γ_{GB} is a function of solute or contaminant composition and compositional gradient then the critical angle to grow from the grain boundary will be less. The result allows the grains to grow in the abnormal growth mode with fewer but larger grains[49,50]. Once the forces on the grain boundary have been released, two dimensional growth models will describe the abnormal grain growth[51-53]. A suggested driving force on the abnormal grain growth is the difference in surface energy of the two neighboring grains, $\Delta\gamma = \gamma_2 - \gamma_1$. The difference could come about from differences in orientation and the compositional differences in the deposited flux on the grain surface. CIGS grains have a preferred growth orientation of <112>. The depositing flux on the surface is composed of four elements at each step in the formation of the CIGS layer. An explanation of the surface energies and surface energy difference due to the deposited flux is beyond the scope of this work.

1.5.1 Sodium Diffusion

The temperature of CIGS deposition is low enough that bulk diffusion is not the dominant method for sodium transport. Grain boundary diffusion is responsible for sodium movement. The sodium referred to is the ion Na^+ that diffuses. Oxygen inclusions in the molybdenum layer are believed to aid sodium diffusion. The oxide formation does not function like a normal oxide of SiO_2 as an example. Transition metal oxides such as MoO_3, V_2O_5, and WO_3 have been investigated for use as thin film batteries. The materials are referred to as bronze compounds with channels that small ions can diffuse through.

The MoO_3 is the cathode and host for lithium (Li^+) intercalcation. Lithium in MoO_3 diffuses in a facile fashion[54]. The chemical nature of sodium is not that far from that of lithium so it follows that sodium should be transported along the grain boundaries in the same manner. The transport of the sodium along the molybdenum grain boundaries has been suggested to follow along the path[55]:

$$MoO_3 + xNa^+ + xe^- \Leftrightarrow Na_xMoO_3 \quad (6)$$

The other less stable molybdenum oxides ($Mo_{1-x}O_x$) act in a like manner[56]. The fast diffusion of sodium is then dependent on the morphology of the molybdenum film. Deposition of molybdenum with electron beam deposition resulted in lower oxygen inclusion than in a sputtered film and less sodium diffusion[57]. The pure molybdenum film did not allow the level of sodium diffusion the sputtered molybdenum layer did. The amount of oxygen needed in the grain boundaries for sufficient diffusion is not known. The transport of sodium depends on the out diffusion from the soda lime glass into the molybdenum, then through the molybdenum before entering the CIGS layer.

1.5.2 Composition Of Soda Lime Glass

Typical glass formers are silicon, barium, phosphorus and arsenic when combined with oxygen, sulfur, tellurium and selenium[58]. The different glass compositions have uses from the common window to lasing elements for neodymium doped glass lasers. The glass compounds can have different chemical reactivities and physical properties. In soda lime glass the silicon oxide makes up seventy weight percent of the glass composition. The

silicon is tetrahedrally coordinated with oxygen. The bond strength is high even in the liquid state for the silicon oxygen bond. Glass composition is tailored to specific process and application requirements. Sodium carbonate is added to assist in mixing of the batch by decomposing to sodium oxide, a flux, and carbon dioxide bubbles which stir the batch[59]. The sodium oxide reduces the melting point and lowers the viscosity of the melt. Limestone (calcium carbonate) and dolomite (magnesium carbonate) are added to make the glass more inert to water. Aluminum, lead and cadmium stabilize the melt and increase the strength of the glass and resistance to chemical attack. Iron, chromium, carbon and sulfur are added to change the color of the glass.

The surface of a soda lime glass substrate is represented in Figure 1-9[21]. The surface has chemisorbed and physisorbed water from the environment. The adsorbed layer is referred to as the gel coat[60]. The gel layer is the onset of corrosion of the surface of the soda lime glass by the cleaning the surface with water[61] at the point of manufacture. For silver mirrors, the soda lime glass surface is prepared by scrubbing the surface with cerium oxide slurry to remove the gel coat[62]. The removal provided for better adhesion of the silver to the glass surface.

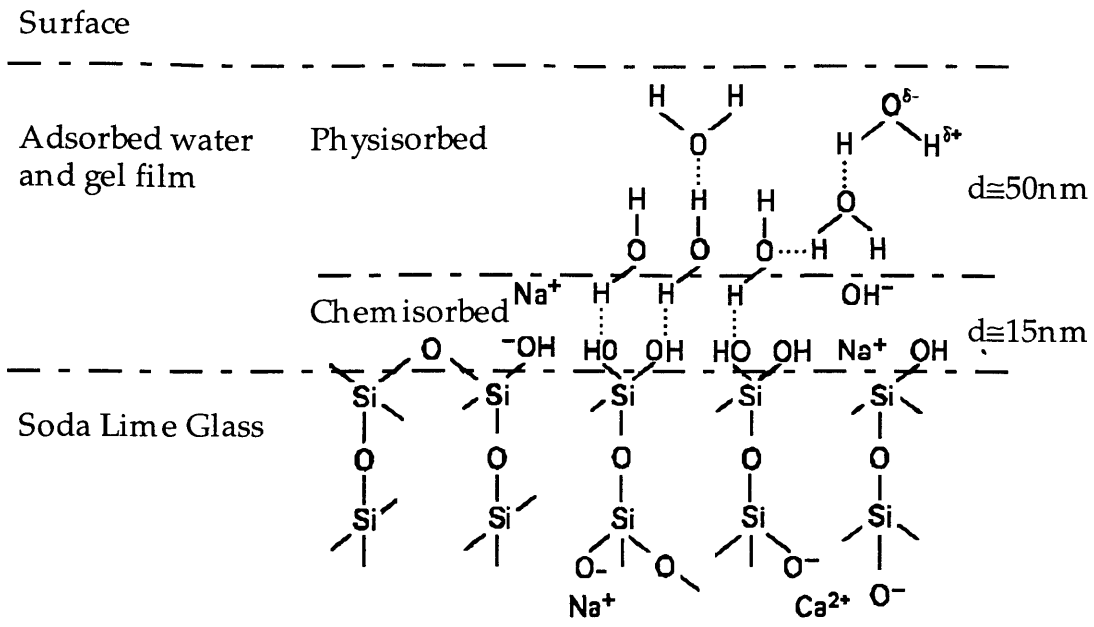

Figure 1-9. Glass surface and adsorbed water layer(gel coat).

1.5.3 Soda Lime Glass Manufacture

Large vats of the glass formulation are made up on the order of thousands of kilograms and then poured out on to a molten tin bath where the glass mixture floats on the surface of the tin. The viscous glass floating on the tin bath over the course of several thousand meters leaves the glass in a uniform thickness and flatness thanks to gravity. The process was developed in 1959 by the Pilkington Brothers of England. There are two sides to the glass now; one side that was in contact with the tin bath and the other side that was exposed to the controlled reducing atmosphere above the float line. The stannous side can be

identified by looking at the glass surface under ultra-violet light where the stannic oxide layer fluoresces by appearing foggy. The estimated thickness of the layer is about 20 μm. The stanate layer is easily removed by polishing . The surface or through an etch process.

2. PROBLEM STATEMENT

The copper indium gallium diselenide (CIGS) photovoltaic cell is made of thin film coatings. The back contact is a 1 μm thick film of molybdenum deposited on a soda lime glass substrate. Essential to the CIGS cell is the adhesion of the molybdenum to the substrate and sodium diffusion through the molybdenum, which enhances the electronic performance. The problem of the molybdenum back contact is the need for optimization of adhesion to the soda lime glass substrate without creating a barrier to sodium diffusion. To address this problem an investigation was performed to examine adhesion and the role the molybdenum coating has on cell performance together with the influence of oxygen in the molybdenum on the transport of sodium.

3. EXPERIMENTAL

The Leybold Hereaus 560 deposition system was employed for this study. The first task in the study was to establish parameters for molybdenum deposition. The parameters that could be controlled were the sputter power, sputter pressure, target to substrate distance and background pressure. Initial work was focused on increasing adhesion of molybdenum to the soda lime glass. Soda lime glass is used as a substrate for copper indium gallium diselenide photovoltaic cells. The substrate must be prepared by cleaning before the deposition of the molybdenum layer can take place. Once cleaned the substrates are loaded into the vacuum chamber for molybdenum deposition. After deposition, the substrates are analyzed for adhesion and then processed into copper indium gallium diselenide cells.

3.1 Materials

Sputter gases were ultra high purity (99.999 weight percent) argon and oxygen supplied by General Air Service and Supply as shown in Table 3-1. The molybdenum target was 99.95 weight percent molybdenum supplied by Plasmaterials of California shown in Table 3-3. The chromium metal supplied by Johnson Mathey was 99.995 weight percent chromium as shown in Table 3-4. The materials used for substrates were soda lime glass manufactured by Pittsburgh Plate Glass or single strength window glass 2.3 mm

thick cut and polished by United States Precision Glass. The other substrate used was a 1 mm thick borosilicate glass manufactured by Corning glass. The composition of the soda lime glass and other substrates was determined as follows. The glass samples for analysis were ball milled to a fine powder, digested in an acid solution and analyzed by Inductively Coupled Plasma(ICP) spectrometry. Table 3-5 shows the results of the elemental analysis for each glass sample. The analysis was performed by Huffman Laboratories in Golden Colorado. The assay was done for elements in the glass considered to be of importance.

As previously discussed, the soda lime glass has two distinct sides, a tin rich and a slightly exposed. The tin layer is roughly twenty microns thick and referred to as the tin side. The top side referred to as the air side is in a reducing atmosphere during the float processing leaving the surface free from tin contamination. Both sides were evaluated in this study. The soda lime glass used in this study had several surface finishes, the as manufactured surface and a cerium oxide polished surface done by the vendor. The polished surface is produced with a cerium oxide slurry on one side of the glass. Substrates with the polishing on the tin and air sides were obtained for molybdenum deposition.

Table 3-1. Listed impurities for ultra high purity grade argon gas supplied by General Air Supply and Service.

Impurity	Guaranteed Specification (molar parts per million)
Water H_2O	<1
Oxygen O_2	<1
Total Hydrocarbon	<1

Table 3-2. Listed impurities for ultra high purity grade oxygen supplied by General Air Service and Supply.

Impurity	Guaranteed Specification (molar parts per million)
Water H_2O	<1
Total Hydrocarbon	<1

Table 3-3. Listed impurities for molybdenum sputter target supplied by Plasmaterials.

Impurity	Guaranteed Specification (molar parts per million)	Impurity	Guaranteed Specification (molar parts per million)
Magnesium	< 10	Iron	< 10
Calcium	< 10	Nickel	< 10
Titanium	< 10	Copper	< 10
Silicon	< 10	Manganese	< 10
Tin	< 10	Aluminum	< 10
Chromium	< 10		

Table 3-4. Listed impurities for chromium supplied by Johnson Mathey.

Impurity	Guaranteed Specification (molar parts per million)	Impurity	Guaranteed Specification (molar parts per million)
Magnesium	< 0.10	Iron	18
Calcium	0.01	Nickel	3.0
Titanium	< 0.10	Copper	< 0.10
Silicon	4.80	Manganese	< 0.10
Oxygen	<5.0	Carbon	10.0
Sodium	< 0.10	Tungsten	<1.20

Table 3-5. Elemental analysis of glass used as substrates.

Measured Element	Soda Lime Glass Pittsburgh Plate Glass (Weight Percent)	Corning 0213, Corning (Weigh Percent)
Aluminum	0.050	1.47
Barium	0.007	0.003
Boron	<0.01	<0.01
Calcium	5.95	0.031
Iron	0.053	0.009
Magnesium	2.27	0.004
Potassium	<0.03	5.10
Sodium	11.1	5.65
Sulfur	<0.1	<0.1
Zinc	<0.001	4.91

3.2 Substrate Preparation

Prior to shipment from the supplier the soda lime glass substrates are washed to remove any particles and grease from the cutting and inspection processes. The substrates are wrapped in tissue paper to prevent scratching during shipping. The tissue paper leaves behind particles that must be removed prior to metal deposition. A simple method of checking surface contamination is with a hand held diode laser. Small particles on the surface scatter light and can be readily spotted through visual inspection.

The glass is cleaned in several steps that have evolved from a simple process including scrubbing, rinse with deionized water and blow dry with nitrogen. In the current cleaning procedure substrates are first scrubbed on both sides and edges with a soft bristle toothbrush with a 1-2 percent solution of Citronox detergent and deionized water. After the scrubbing the substrate is loaded into a substrate carrier submerged in the detergent solution. The substrates are moved and sonicated in a heated 1-2 percent solution of Citronox detergent bath for thirty to ninety seconds. The Zenith ultrasonic tank used operates at 80 kilohertz with a maximum ultrasonic power of 600 watts. The bath temperature is held at 70 degrees Celsius. The substrates are rinsed with deionized water then sonicated with heated clean deionized water for thirty to ninety seconds. During the cleaning process the substrates are kept submerged at all steps to not allow any drying of the substrate and water spot formation. The final rinse and dry is done by a Semitorr spin rinser-dryer. Here substrates are rinsed with heated deionized water for two hundred seconds at eight hundred rotations per minute and the rinse water reaches fifteen megohms of resistivity. The spin dry cycle follows with flowing heated nitrogen for four hundred

seconds at twenty five hundred rotations per minute. The substrates are then immediately placed in the deposition system.

3.3 Molybdenum And Chromium Film Deposition Procedures

Thin film deposition for this study was done with physical vapor deposition techniques. A vacuum chamber is used to provide a controlled environment and to isolate the vaporized materials from contamination. Both depositions were performed in-situ so as to maintain a clean interface. Two different methods of deposition were used. The chromium was deposited by the electron beam method because of the ability to controllably produce thin layers in the system. Sputtering is used for the deposition of one micron thick molybdenum films because of suitability to coat large area thick film deposition.

3.3.1 Deposition Apparatus

Molybdenum and chromium deposition were performed in a Leybold Hereaus 560 deposition system. The vacuum chamber is evacuated by a Leybold TMP 1500 turbo pump. The molybdenum was sputtered from a 150 mm diameter DC magnetron. The DC power supply is rated to eighteen hundred watts and used in the constant power mode. A shield wall separates the electron beam source and the DC magnetron sputter cathode. The rotation speed of the platen has three fixed speeds. The substrates were mounted to the underside of the rotating platen in a sputter up configuration. The resulting translation speed of the substrates past the DC magnetron was measured to be 0.56, 11 and 174 mm/second. The location of the DC magnetron is centered under and set at 70-75 mm

distance from the path the substrates follow. Figure 3-1 shows a schematic of the chamber layout.

Sputtering of molybdenum requires a constant pressure of several mTorr. The pressure was set by flowing argon into the chamber. The throttle valve was used to limit the fifteen hundred liter a second pumping capacity of the turbo pump. The flow rate of the argon was controlled by a MKS Instruments 0-100 sccm mass flow controller and the oxygen flow with a 0-10 sccm mass flow controller. The chamber pressure was monitored with a MKS Instruments, high accuracy heated, 627 Baratron gauge accurate to 0.1 mTorr.

3.3.2 Chromium Deposition

The Leybold system is equipped with a five kilowatt electron beam source and four pocket hearth that was used to deposit chromium. The electron beam unit is mounted to the bottom of the deposition chamber with a separation distance to the substrates of 360 mm. The deposition is controlled by a programmable Inficon IC6000 controller. The controller uses a crystal rate monitor to measure deposition rate, which is compared to the programmed rate to control the electron beam power. The programmer is set for desired film thickness and rate by the user. The chromium was deposited at a rate of 1 nm a second for the films greater than 10 nm thick. For films less than 10 nm thick, a rate of 0.5 nm a second was used.

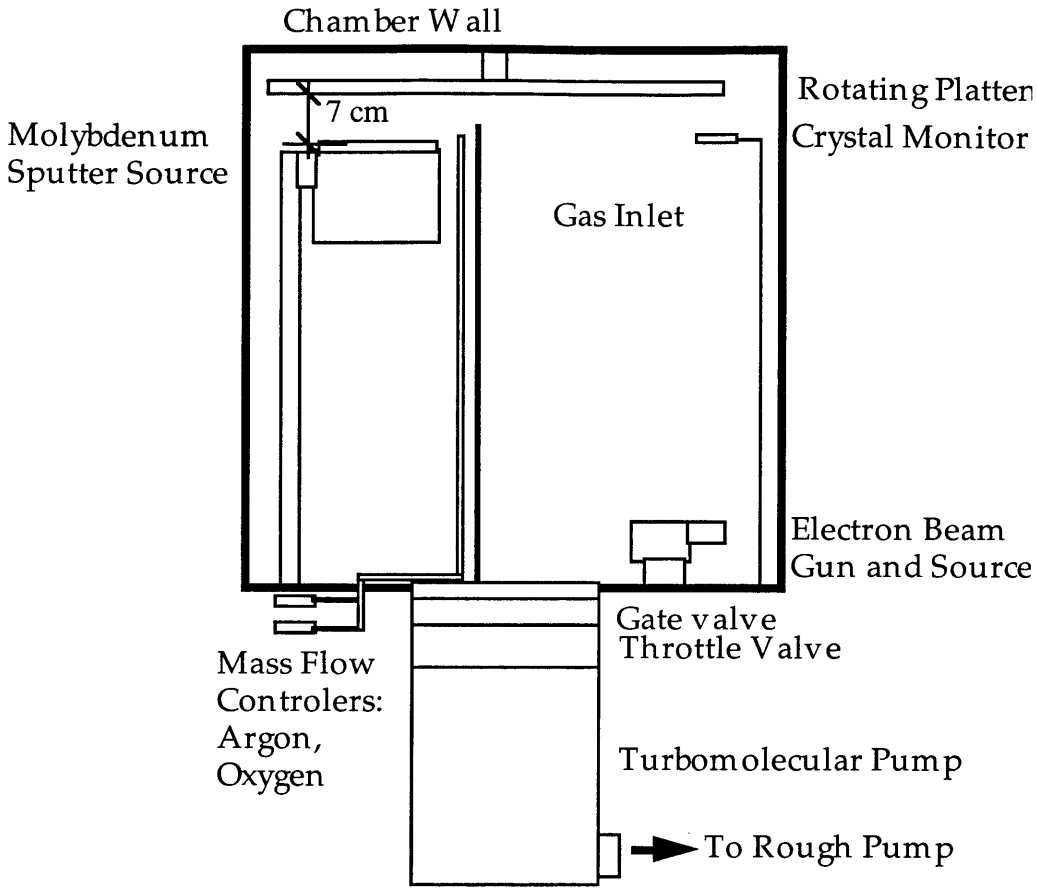

Figure 3-1. Leybold Hereaus 560 Deposition System. The rotating platen is suspended from the top of the chamber and the substrates are mounted to the bottom side. Deposition is then accomplished by positioning the substrate over the DC magnetron or electron beam gun and source.

The Inficon IC6000 was programmed with the density and tooling factor for chromium. The measured thickness was calibrated by depositing a chromium film and comparing the programmed thickness to the actual thickness as measured by the Sloan Dektak[3] profilometer to obtain the tooling factor. The tooling factor is entered into the controller and a chromium film deposited and the thickness is checked. The iterative process of thickness correction produces an accurate deposition thickness.

The background pressure was $1x10^{-6}$ Torr before deposition was started. The controller was programmed for a two minute ramp up to six percent power that equates to a deposition rate of 1 nm/second. The electron beam power supply voltage was 10.7 kilovolts and electron beam current of 15 milliamperes. Following the ramp period the shutter is automatically moved from over the electron beam unit and the controller establishes a control loop by monitoring the deposition rate and controlling power. The shutter is automatically closed when the programmed thickness value is reached.

A calibration run was performed first with the substrates moved out of deposition range. The electron beam alignment on the chromium and deposition rate stability were checked. The calibration chromium deposition getters contaminants in the chamber typically lowering the system pressure down to $4x10^{-7}$ Torr. Allowing for the chromium film to be deposited with less contamination from the deposition system. The platen was rotated to move the substrates over the electron beam unit and the programmed chromium thickness was deposited. The substrates then were ready for deposition with molybdenum. The system pressure does increase to the initial base pressure after a few minutes as gas trapped in the built up metal layers on the chamber walls evolves.

3.3.3 Molybdenum Deposition

Clean substrates are use loaded into a holder and the holder is affixed to the underside of the platen. The chamber is evacuated to a base pressure of 1 x 10^{-6} Torr. The Baratron gauge is zeroed. With the throttle valve fully engaged the desired sputter pressure range of 1-10 mTorr could be attained with flow rates from 3 to 30 sccm of argon. The DC power supply is operated in the constant power mode and set at 750 Watts. The sputter discharge voltage was measured by the power supply and depending on system pressure varied between three hundred and three hundred eighty volts. The substrates are shielded from the DC magnetron when power is applied to the DC magnetron. The molybdenum is presputtered for three minutes before the substrate translation at the lowest setting is started (0.56 mm/second). The fixed rotation speed of the platen necessitates that sputter power to be changed for a specified thickness. Multiple passes can be made to accomplish the correct thickness for low sputter rates.

3.3.4 Oxygen Addition To Molybdenum

The effect of adding oxygen during sputtering of the molybdenum film was explored. Studies for similar metals[63] have shown oxide formation during sputtering at the grain boundary. The oxide structure is larger than the molybdenum structure causing the grains to push on each other. A compressive stress component would result, relieving some of the tensile stress in the typical film. A zero to ten cubic centimeter a minute (sccm) mass flow controller was used to control oxygen flow during sputtering. Four oxygen amounts were added: 0.5, 1, 1.5 and 2 sccm with the flow of argon adjusted to maintain a total

pressure of 4 mTorr. The sputtering was done in the same manner as described in the molybdenum sputtering section.

3.3.5 Residual Stress

The deposition of molybdenum results in residual stress in the thin film. By using delicate 50.8 mm x 50.8 mm x 0.2 mm glass substrates the gross residual stress of the molybdenum film could be determined. Compressive stress in the film causes a convex bow in the substrate. Tensile stress caused a concave bow in the substrate. This observed behavior is a simple qualitative test for residual stress, and the substrates must be handled carefully. No quantitative measurements of the bowing relative to stress have been made,

only gross observations as reflected in Table 3-6. The substrates showed some biaxial stress irregularities. The substrate bowed the most in the axis perpendicular to rotation. Non-uniform bowing in perpendicular directions indicates biaxial stress and has been seen in other work [64].

Table 3-6. Visual inspection results of 50 mm x 50 mm x 0.2 mm glass substrates.

Sputter Pressure (mTorr)	Power (watts)	Intrinsic Stress (observed)	Sheet Resistance (Ω/□)
4	750	Tensile	0.095
5	750	Tensile	0.097
6	750	Tensile	0.097
7	750	Compressive	0.104
10	750	Compressive	0.134

3.3.6 Surface Treatments To Increase Adhesion

Another approach to improve adhesion besides the use of chromium was to pre-etch the soda lime glass surface. During the substrate cleaning procedure after the scrubbing and rinsing, the substrates were etched in a ten percent hydrofluoric acid solution. The etching was found to remove an average of 61 nm a second as shown in Table 3-7 . The etching is done under ultrasonic agitation to improve the etch uniformity at the surface. Stirring of the solution while etching was not attempted. Once etched the substrates were placed in a deionized water cascade rinse tank for fifteen minutes to remove any residual acid. The

substrates were then loaded into the spin rinser/drier for the same cycle used with the normal cleaning procedure. The substrates were then loaded into the vacuum chamber for molybdenum deposition.

Table 3-7. Hydrofluoric acid etch results.

Etch time in seconds	Measured depth(mm)	Etch rate per second(nm)
15	0.9108	60.7
30	1.832	61.0
45	2.782	61.8
60	3.833	63.8
75	4.778	63.7

3.4 Measurement, Analysis Apparatus And Procedures

All measurements and analysis were performed at the National Renewable Energy Laboratory in Golden Colorado except for the assay of the substrates which was done at Huffman Laboratories, Inc. of Golden Colorado.

3.4.1 Sheet Resistance And Thickness Measurements

The sheet resistivity ρ_s of thin films was measured with a collinear four point probe array shown in Figure 3-2. The spacing between the probes is equal distant. The four point probe is made by Kulicke and Soffa Industries with a probe spacing of 0.625 mm. The tungsten carbide probes are spring loaded to 75 grams to make repeatable measurements. A model 225 Keithley constant current source supplies current through the outer two probes. The measurement is simplified by setting the current supply to 4.53 milliamperes then the sheet resistance is displayed directly by the voltage meter. The voltage is measured across the center two probes by a Fluke 8840A multimeter. The sheet resistance can be calculated following the American Standards Testing Materials procedure F390-78[65]. Equation 1 was used to calculate sheet resistance.

$$\rho_s = 4.53(\text{Volts}) \div (\text{Amps}) = \text{ohms/square} = (\Omega/\square) \tag{7}$$

Sheet resistance is measured in Ohms with the unitless square term as a reference to the geometrical relationship to used calculate the resistance of an interconnect on an integrated circuit.

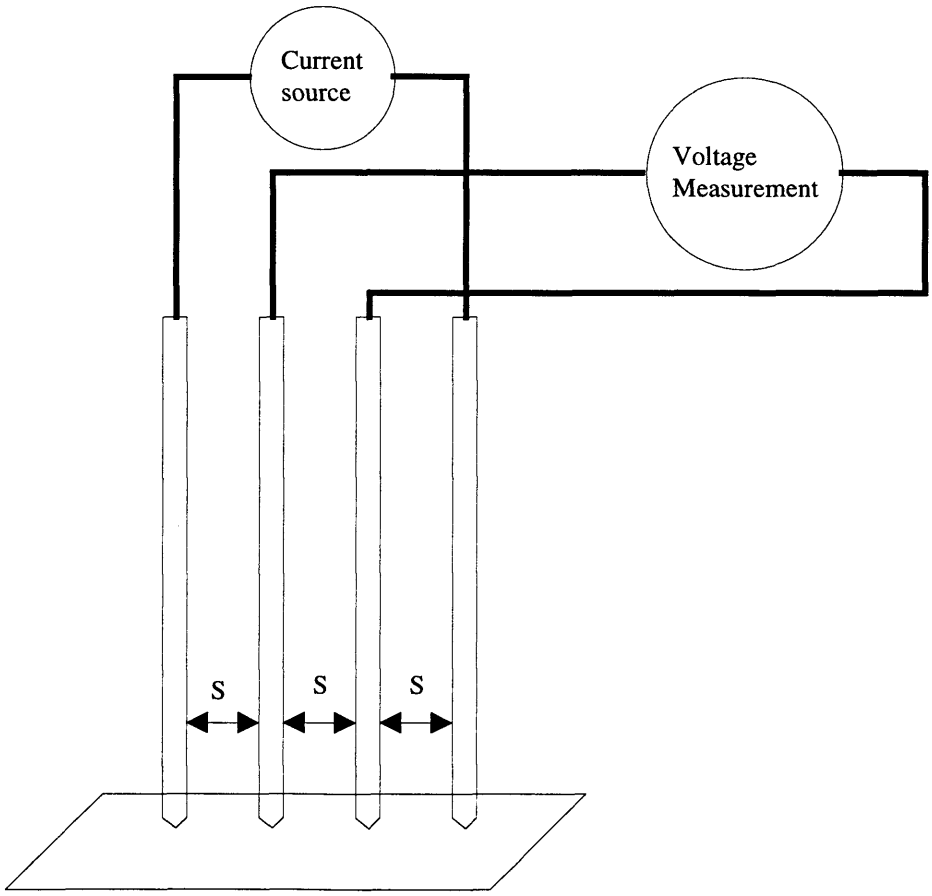

Figure 3-2. Four point probe used to measure sheet resistance.

3.4.2 Film Thickness Measurement

Film thickness was measured with a Slone Dektak[3] step profilometer. The measurement is performed under computer control and uses a software leveling and measurement. The profilometer is calibrated using reference standards supplied by the manufacturer. Two methods were used to produce a step for measurement. Titanium dioxide powder was mixed with isopropyl alcohol to a paint consistency and applied in a two millimeter dot to the surface of the substrate prior to molybdenum deposition.

The titanium dioxide is heat resistant and masks the surface and is removed from the surface after deposition by rinsing with water. The step formed by the titanium dioxide is rough around the edges and the repeatability of the measurement is within ± 20 nm for each hole in the molybdenum. For the molybdenum film the accuracy is acceptable. To resolve a 10 nm chromium film on a glass surface of comparable surface roughness with the profilometer is difficult. The second method employed was the liftoff photolithographic technique. A microscope cover slide is coated with photoresist and patterned leaving fifty micron wide lines exposed on the glass surface. The chromium is deposited and then the photoresist removed with acetone leaving only the exposed pattern. The chromium line is then measured with the Sloan Dektak[3]. The photolithography method is sensitive to heat over 130°C and is therefore not compatible with one micron thick molybdenum deposition.

3.4.3 Compositional Measurement

The copper indium gallium diselenide cells were profiled with secondary ion mass spectrometer (SIMS). The Cameca system uses an ion beam of cesium to sputter the sample and the ejected atoms are measured with a mass spectrometer. The following isotopes were measured by the system to profile the copper indium gallium diselenide cells and are given in Table 3-8.

Table 3-8. Atomic masses followed by elemental SIMS analysis to profile CIGS cell.

Element	Atomic Mass	Element	Atomic Mass
Mo + Cs	92 + 133	Ga + Cs	71 + 133
Na + Cs	23 + 133	Se + Cs	82 + 133
Cu + Cs	63 + 133	In + Cs	113 + 133

3.4.4 Imaging

Cross sectional imaging was performed on a Jeol 6320F field emission scanning electron microscope with a spatial resolution of 1.2 nm at 20 kilovolts. The samples are fractured to produce a sharp edge and mounted on a aluminum sample mount with conducting carbon paint. The mounted sample is then loaded into the SEM for imaging.

3.4.5 Structural and Stress Measurements

X-ray diffraction analysis was used to characterize the structure and stress in the molybdenum films. A Scintag four circle x-ray diffraction system is used to make the measurements. The x-ray source is a copper tube and the wave length used is the $K_{\alpha}1$. The x-ray source is operated at forty five kilovolts and forty milliamperes. A two millimeter pinhole collimator is mounted to the x-ray tube to focus on the sample. The detector has 200 mm Soller slit to focus the reflected beam to the solid state detector. The system is calibrated weekly with a traceable NIST standard. A long scan is performed using the $\theta/2\theta$ Bragg angle diffraction method to measure all of the known peaks. A texture measurement called a pole figure assumes a film is made up of tiny crystals and measures the orientation of the crystals in relation to each other[66]. The pole figures measured are of the crystal orientation (110) plane which occurs at 2θ equal to 40.516 degrees. Residual stress is measured in the film by looking at the shift in a high angle peak as the sample is angled[67-70].

3.4.6 Adhesion Testing

The adhesion of the molybdenum was tested with a simple tape pull test. The tape used was Scotch 810 Magic tape manufactured by the 3M company. Previous experience demonstrated that if the molybdenum could not be pulled off with a pressure sensitive tape adhesion would survive the deposition process[64]. The test is performed with a new piece of tape 100 mm long applied across the middle of the substrate. The tape is rubbed down to assure maximum adhesion to the molybdenum surface. The substrate is held firmly on a flat surface. The tape is then pulled off quickly at an angle normal to the surface of the substrate.

Table 3-9. Scotch 810 Magic Tape Description

Backing:	Matte Acetate
Adhesive:	Synthetic
Adhesion to Steel	25 oz./in. width
Tensile Strength:	15 lb./in. width

3.5 Annealing

The first sample set for adhesion testing was annealed in a 60 mm diameter quartz tube furnace. The tube was purged with argon during anneal to limit possible oxide formation on the molybdenum film. A Lindberg clam shell furnace was located at the middle of the tube so the sample could be loaded in a cool zone and purged before introduction into the hot zone. The annealing profile was five hundred thirty degrees Celsius for fifteen minutes. The substrates were then removed from the hot zone to cool in the flowing argon.

3.6 Atomic Force Microscopy

A Park Scientific Instruments Autoprobe AFM/STM was used for the surface roughness measurements. The atomic force microscope can make roughness measurements on non conduction substrates. The ability to image the surface was not used for this work.

3.7 Growth And Characterization Of CIGS Films

The CIGS cells were fabricated at the National Renewable Energy Laboratory using the three stage method[2,8,71]. The method uses co-evaporation of elemental sources in a diffusion pumped chamber. An $(InGa)_2Se_3$ layer is grown at 250° Celsius then the temperature is ramped to 550° Celsius in the presence of selenium vapor then copper is evaporated. Last the limited amounts of gallium and indium are evaporated to convert the film to copper deficient. The temperature was then ramped down to 300° Celsius in a

selenium vapor atmosphere. The CIGS film cools to room temperature. CdS is deposited on the CIGS layer by an aqueous chemical bath deposition[11]. The ZnO was deposited in two layers; first the intrinsic layer deposited by RF magnetron sputtering with a partial pressure of oxygen. Second the conducting aluminum doped ZnO layer was sputtered using an RF magnetron. Shadow masks were employed during the aluminum and nickel evaporation to pattern grids on the ZnO layer. Current-voltage (I-V) measurements were performed under global air mass (AM) 1.5 insolation. The cells are mounted to a water cooled plate maintained at 25° C. A Keithley instruments 238 High Current Measurement Scanner scans voltage from -0.5 to 1.0 Volts while monitoring current. The area used to calculate efficiencies is the total area including the grid area. The cells were measured for efficiency (η), open circuit voltage (V_{OC}), short circuit current (J_{SC}) and fill factor (FF).

4. RESULTS AND DISCUSSION

This section is divided into two parts. The first part discusses the exploration of parameter space for the sputter deposition of molybdenum in the Leybold Hereaus deposition system employed in this study. This includes adhesion improvement with a thin layer of chromium deposited between the soda lime glass and the molybdenum film. It also includes an investigation of the etching of the soda lime glass to get away from requiring a chromium layer. The molybdenum films were analyzed and compared to a baseline process used at National Renewable Energy Laboratory for high efficiency CIGS cells.

In the second part of the section, the addition of oxygen to the molybdenum sputtering process will be reported. The influence of oxygen addition during deposition, thought to affect grain boundary transport of sodium, was examined. SIMS was used to analyze the diffusion of sodium through the molybdenum layer and into the copper indium gallium diselenide layer. Device conversion efficiency measurements were performed and the results were compared to baseline results. The change in structure and residual stress in the deposited molybdenum films was investigated by x-ray diffraction analysis.

4.1 Sputtered Molybdenum Films

The Leybold Hereaus deposition system is capable of coating multiple substrates at a time. The goal was to have a 1 μm thick molybdenum film deposited in a single pass of the substrate across the DC magnetron. The matrix shown in Table 4-1 was designed to cover the range of sputter pressure 2 to 7 mTorr and sputter power from 350 to 900 watts. The pressure range was chosen from previous studies at the National Renewable Energy Laboratory[64]. The low sputter power deposition would not achieve a thickness of 1 μm in a single pass so multiple passes were made. The soda lime glass substrates were cerium oxide polished on the air and tin sides to facilitate testing for adhesion differences between the two sides. The molybdenum film was then tested for adhesion to the soda lime glass with the tape pull test. The results of the adhesion test for the molybdenum to the two sides of the soda lime glass substrate are shown in Table 4-2 and Table 4-3.

Table 4-1. Matrix of sputter parameters to test adhesion of the molybdenum film to soda lime glass. Specimen numbers are indicated.

Pressure Power (Watts)	2 mTorr	3.5 mTorr	5 mTorr	7 mTorr
350	950908	9509011	950912A	950912B
625	95919B	95918A	95919A	95915B
900	95913A	95914A	95913B	95915A

Table 4-2. Tape pull test results of molybdenum adhesion to the air side of the soda lime glass substrate.

Pressure Power (Watts)	2 mTorr	3.5 mTorr	5 mTorr	7 mTorr
350	pass	pass	pass	fail
625	fail	pass	pass	pass
900	pass	pass	pass	fail

Table 4-3. Tape pull test results of molybdenum adhesion on tin side of the soda lime glass substrate.

Pressure Power (Watts)	2 mTorr	3.5 mTorr	5 mTorr	7 mTorr
350	pass	pass	fail	fail
625	pass	pass	pass	fail
900	pass	pass	pass	pass

From the results in Table 4-2 and Table 4-3 molybdenum adhesion does not show a preference for better adhesion to the air or tin sides of the soda lime glass substrate. The tape test does not reveal a clear pattern for failure when comparing both tables. If the tin side of the substrate results are evaluated. The conclusion would be increased power and lower sputter pressure results in good adhesion.

To approximate the CIGS deposition process temperatures, the samples were subsequently annealed at 530° C in a tube furnace in flowing argon. After anneal the samples appeared darker, suggesting oxidation of the molybdenum surface of the film occurred. Molybdenum typically forms oxides of composition MoO_2 and MoO_3 as low as 250° C[72-74]. The tube furnace purge duration was increased and did not substantially change the appearance of the films. The majority of the samples failed the post anneal adhesion tape pull test as shown in Table 4-4 and Table 4-5.

The failure after the annealing step indicates that the film adhesion is complicated. The likely reason for the high failure rate of the tube furnace annealed samples is due to the thermal shock the substrate experienced when inserted into the hot zone of the tube furnace (at an estimated ramp rate of 180° C per minute). The substrate would typically experience 60° C per minute ramp during the normal CIGS deposition process. Annealing under atmospheric pressure may also be different than annealing under vacuum.

Table 4-4. Tape pull test of post annealed molybdenum films on the air side of the soda lime glass substrate.

Pressure Power (Watts)	2 mTorr	3.5 mTorr	5 mTorr	7 mTorr
350	fail	fail	fail	fail
625	fail	fail	fail	fail
900	fail	pass	fail	pass

Table 4-5. Tape pull test of post anneal molybdenum films on the tin side of the soda lime glass substrate.

Pressure Power (Watts)	2 mTorr	3.5 mTorr	5 mTorr	7 mTorr
350	fail	fail	fail	pass
625	fail	fail	fail	fail
900	pass	fail	fail	fail

The thickness measurements from each of the samples shows that the deposition rate is not pressure dependent in the range used in this study as shown in Figure 4-1. From the thickness data the sputter power required to deposit a1 μm thick molybdenum film in a single pass was calculated. The thickness was plotted and the intercept for 1 μm was at 700 Watts as shown in Figure 4-2. To ensure the film was at least 1 μm thick, the sputter power was increased to 750 Watts . The calculated thickness for a film sputtered at 750 watts is 1.02 μm. The measured film thickness was 1.1 μm.

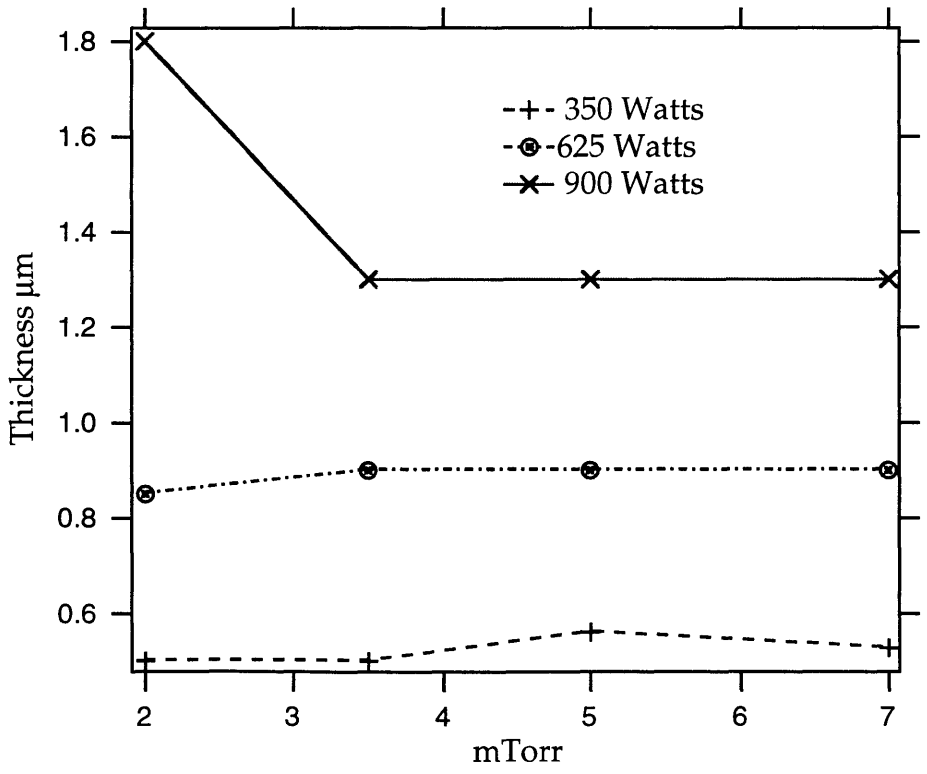

Figure 4-1. Film thickness as a function of sputter pressure.

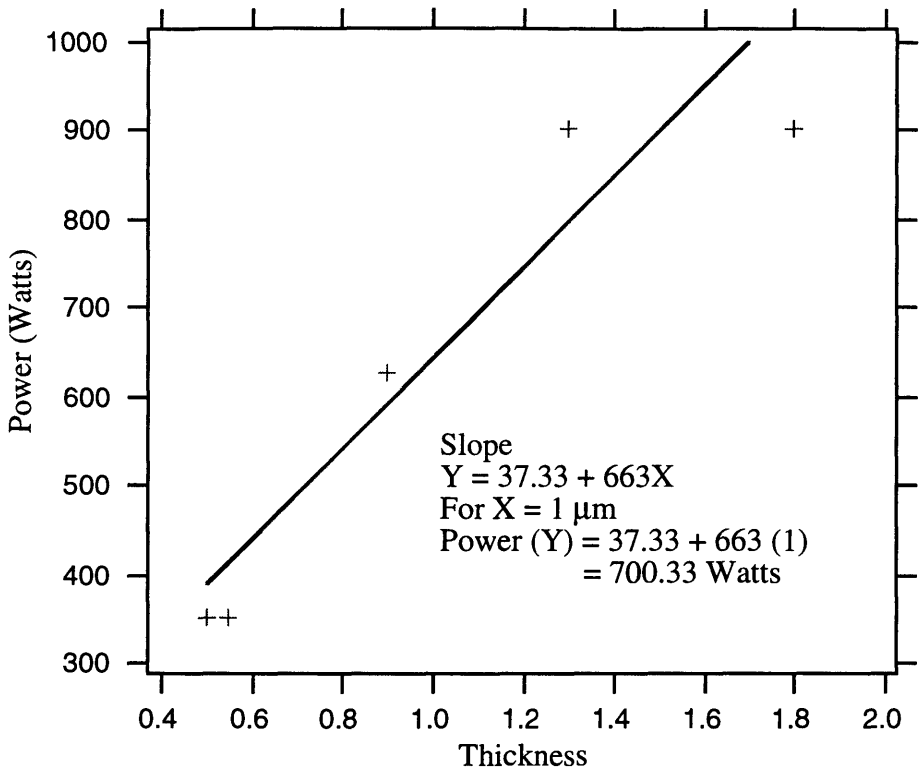

Figure 4-2. Molybdenum film thickness for a single deposition pass by the DC magnetron as a function of sputter power.

4.1.1 Molybdenum Film Morphology

A cross section SEM micrograph of the molybdenum film and the initial part of the CIGS layer is shown in Figure 4-3. The columnar growth of the molybdenum characterizes the growth as typical for that in zone 1 from the Thornton diagram[31]. The curved grains are found along the translation direction the of the substrate during deposition and are not observed if the substrate is cleaved perpendicular to the translation direction. The translation of the substrate affects the grain growth at the start of the molybdenum film formation. The incidence angle from the sputter cathode to the substrate surface is oblique. The particle flux is not as energetic and the first layers are shadowed heavily because of the low angle. The sputtered particles do not impact with enough energy to have any surface mobility causing the growing film to be porous. The molybdenum film at the beginning and end of growth (where there is also a low angle of incidence) contains a large amount of trapped gas atoms, most likely due to void networks generated as by the shadowing models proposed by Muller and others[32,33,75,76]. Directly over the DC magnetron the grains grow normal to the surface of the substrate. In the illustration of Figure 4-4 the grains grow towards the direction of the DC magnetron.

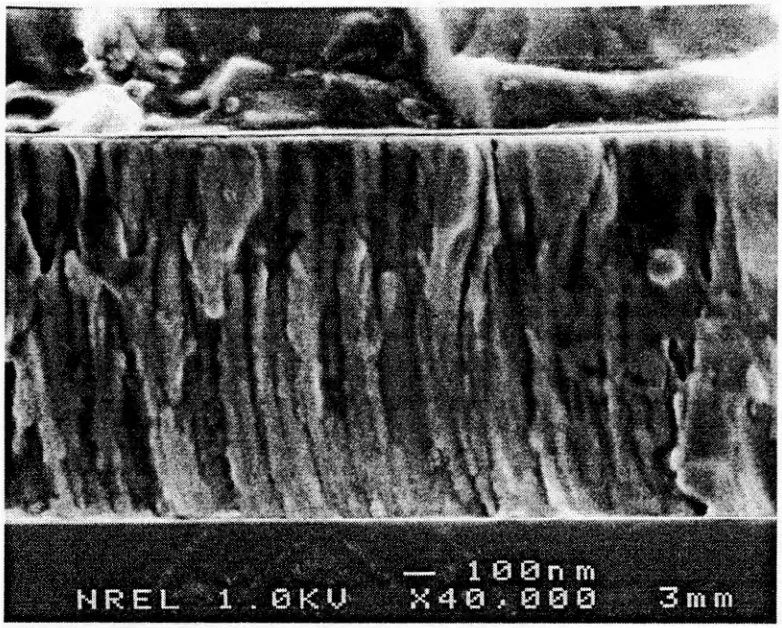

Figure 4-3. 1 μm Molybdenum film deposited at 4 mTorr and a sputter power of 750 Watts.

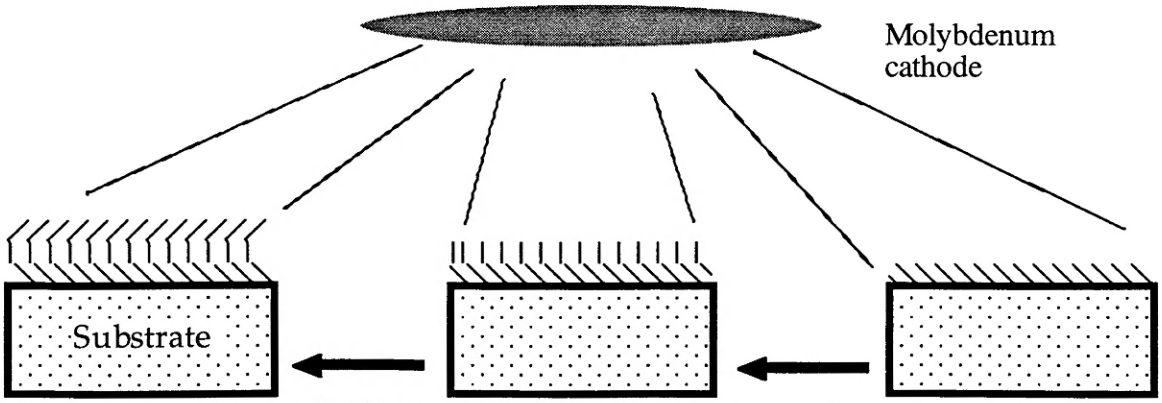

Figure 4-4. Directional effects on molybdenum grain growth as the substrate is translated past the molybdenum cathode.

4.1.2 Summary Of Sputtering Parameters

The sputtered molybdenum films show an increase in adhesion with increasing sputter power. The adhesion of the molybdenum was shown to be equal on both sides of the soda lime glass. The thickness of the molybdenum film can be controlled effectively by raising the sputter power. The grain growth for the molybdenum film exhibits zone 1 growth from the Thornton diagram. The translation of the soda lime glass substrate past the DC magnetron induces preferential grain growth in the direction of the translation. The beginning and end of the molybdenum film growth regions are porous and have larger amounts of trapped gas atoms due to the low angle of the deposition flux caused by the substrate translation.

4.2 Adhesion Promotion

The poor results of the sputter parameter optimization (especially after anneal) lead to attempts to improve the adhesion. Two approaches were attempted. The first approach was to put a chromium interlayer down in a method similar to that utilized by the semiconductor industry. The second approach tried to capitalize on the fact that many times a mechanical bond can be improved by a rough surface and etching of the glass surface to increase surface roughness might improve the molybdenum/soda lime glass interface adhesion.

4.2.1 Chromium Interlayers

Reactive metals like titanium and chromium are used as adhesion promoters for contacts on semiconductors. The reactive metal is capable of reacting with an oxide surface and bonding or alloying with the metal as well. In work not reported here interlayers of titanium were found to promote adhesion. The titanium was able to diffuse into the CIGS layer during growth and be detrimental to cell efficiency. Chromium was selected over titanium because of the ease of deposition with the electron beam process. Chromium also getters contaminants in the vacuum chamber during evaporation. The background pressure of the chamber typically drops from $1.0x10^{-6}$ to $7.0x10^{-7}$ Torr by evaporating chromium onto a shutter prior to depositing the chromium adhesion layer. After chromium deposition the molybdenum was immediately sputtered onto the chromium layer. The air side of the soda lime glass substrate was used for the chromium depositions. The pressure for the molybdenum layer was varied from 3 to 7 mTorr of argon pressure and the sputter power remained constant at 900 Watts.

The results in Table 4-6 show chromium layers from 2.3-59 nm improved adhesion effectively. The films were subsequently annealed in vacuum following the profile used for CIGS [71] deposition shown in Figure 4-5. The only film that failed was the deposition that did not have a chromium layer. The effect of the chromium on adhesion was positive, even for the thinnest chromium layer of 2.3 nm, the all the molybdenum films passed the tape pull test. The change in sputter pressure for the different depositions did not affect the adhesion of the molybdenum. The residual stress of the molybdenum film was not measured but assumed to change as has been reported[64].

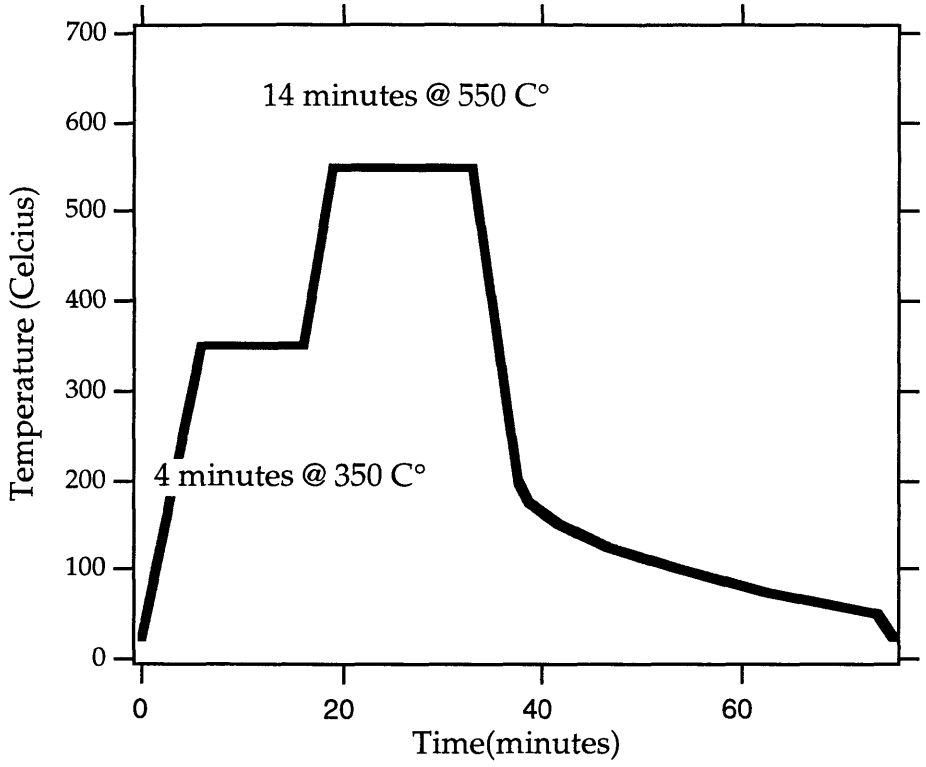

Figure 4-5. Annealing profile for samples in the copper indium gallium diselenide deposition system.

Table 4-6. Adhesion results for molybdenum films with a chromium interlayer deposited on the air side of the soda lime glass substrates.

Sample	Pressure (mTorr)	Power (watts)	Chromium (nm)	Tape test	Post Vacuum Anneal Tape test
951102	3	900	0.0	pass	fail
951023A	7	900	2.3	pass	pass
951018B	7	900	6.5	pass	pass
951102	3	900	6.5	pass	pass
951019A	7	900	10.8	pass	pass
951016	5	900	40.0	pass	pass
951017A	5	900	59.0	pass	pass

Use of the chromium would allow for a increased range of parameters to be used for sputtering. The sputtering variables could change and not affect adhesion of the molybdenum with the use of chromium.

Table 4-7 shows the effects of sputtering pressure on the film resistance for a molybdenum thickness of approximately one micron with a chromium adhesion layer. The bulk resistivity of molybdenum is 5.7 μohm-cm[77]. The lower sputter pressures produce sample resistivities approaching the bulk resistivity of molybdenum within a factor of two. After anneal the sheet resistance was measured and a drop in the resistivity can be seen in all but one sample. The transmission of a lateral current through the molybdenum is complicated. The cross section of a grain is 100 nm in diameter so the number of grains to cross is large. The drop in sheet resistance could be due a change in the molybdenum stress state, impurities at the grain boundary, and to grain boundary passivation.

After anneal small parallel cracks were observed in the two substrates sputtered at 3.2 and 7.5 mTorr. The presence of the small, linear parallel cracks is typically observed on well adhered molybdenum on soda lime glass. The cracks are seen when the substrate is heated above the softening point of the glass. The molybdenum is under tensile stress from the soda lime glass expansion and the film pulls apart in a linear fashion. Bowing of the substrate occurs during the softening of the glass, where the glass is forced to bend by the molybdenum film. The substrate remains bowed after cooling[78]. The other form of cracks sometimes found in the molybdenum films occurs when the soda lime glass cools. The molybdenum film is put under a large compressive stress. The stress is sufficient to force the molybdenum film to buckle forming non-linear cracks on the surface.

Table 4-7. Effects of sputter pressure on molybdenum/chromium sheet resistance.

Sample	Pressure (mTorr)	ρ_s (Ω/□)	Molybdenum Conductivity (μohm-cm)	Post Vacuum Anneal Molybdenum Conductivity (μohm- cm)
951113	0.75	0.16	16	16
951109	1	0.18	18	11
951108	1.8	0.2	20	18
951102	3.2	0.35	35	26
951104	7.5	0.7	70	45

There is some uncertainty about the anneal temperature of the substrates in the CIGS system because the temperature sensor is not in direct contact with the substrate surface. The temperature is calibrated to establish a correction temperature curve. The correction temperature curve is used to determine the substrate temperature from a probe in close proximity. Changes in the absorption/eminence of the temperature probe can give a ten degree Celsius temperature swing. When the temperature probe is calibrated properly the softening point of the soda lime glass is not reached and the cracking and bowing do not occur.

4.2.2 Device Performance

Devices were fabricated by the standard CIGS method on soda lime glass substrates only with molybdenum and molybdenum with chromium interlayer. A comparison of conversion efficiency of shows a distinct difference. Open circuit voltages have been demonstrated by others to be sensitive to reduced sodium[3]. In Figure 4-6 and the current voltage curve measurements for two representative CIGS cells are shown. The dashed trace represents a cell with no chromium interlayer, a slight difference in V_{oc} is observed. The difference is about fifty millivolts and is typical of cells made with the chromium adhesion layer. The suspected cause behind the difference is a decrease in the amount of sodium diffusing through the chromium layer to the CIGS layer during growth. This decrease may be caused by the presence of chromium oxide in the interlayer.

4.2.3 Sodium Diffusion

Although not fully understood, sodium is very important to the production of high efficiency CIGS devices. The primary sodium source is the soda lime glass substrate. Thus, sodium levels through the molybdenum film after anneal were investigated by elemental SIMS depth profiling of samples with and without chromium interlayers as shown in Figure 4-6. The sodium level in the molybdenum film with the chromium layer is below the amount found in the corresponding layer of the other sample with out a chromium layer. The difference is nearly a factor of two. The oxygen level is also seen to be lower in the molybdenum film with the chromium interlayer. The lowered oxygen

Table 4-8. Peak efficiency measurements for the two cells one with and one without a chromium layer shown in Figure 4-6.

Sample	V_{oc} (Volts)	I_{sc} (ma/cm^2)	Efficiency %	Fill Factor %
Control no Chromium	0.607	29.85	13.205	74.14
Chromium layer	0.549	29.35	11.287	68.91

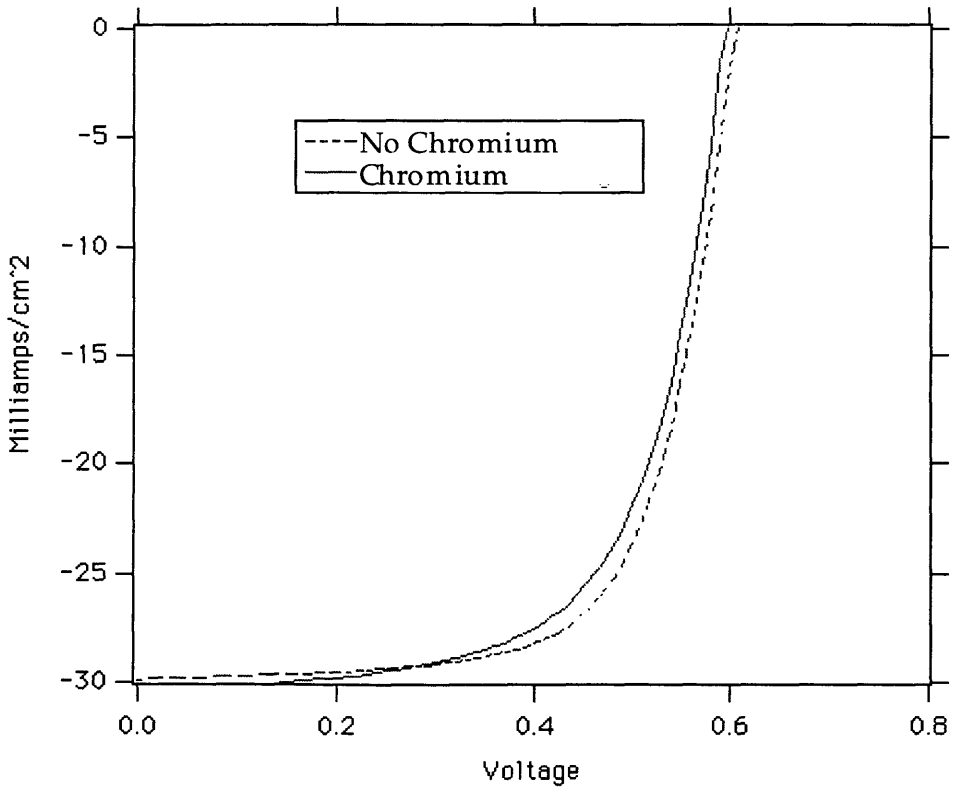

Figure 4-6. IV comparison of two CIGS cells with and without chromium interlayers.

content of the film results from the oxygen gettering that occurs before and during deposition of the chromium layer. The amount of sodium in the molybdenum film is closely correlated to the oxygen level of the film. The oxygen is thought to be found in voids and grain boundaries, where some of the oxygen will react with the molybdenum during sputtering to form several phases of $Mo_{1-x}O_x$[79]. The most stable oxide MoO_3 will react with the sodium ion Na^+ as shown:

$$MoO_3 + xNa^+ xe^- \Leftrightarrow Na_xMoO_3 \text{[55]} \quad (8)$$

Electrochromic films of MoO_3 reversibly intercalate lithium ions and the lithium ions have diffusion rates D_{Li+} on the order of 10^{-12} cm^2/s at a temperature of 120° C[54]. It follows that the sodium can readily diffuse along the MoO_x sites during an anneal.

The SIMS sodium profile shown in Figure 4-7 does not show a concentration gradient across the molybdenum film that would be indicative of a limited diffusion profile. The sodium shows an increase in concentration at the molybdenum/soda lime glass interface where oxygen concentration is high. The high oxygen concentration at the interface occurs in voids where the molybdenum is starting to form grains on the surface of the soda lime glass. The amount of oxygen trapped in the molybdenum film depends on the residual background pressure of the deposition system and the sputter power used for deposition. Oxygen content has been shown to decrease with increasing sputter power[79]. The SIMS experiment cannot evaluate the kinetics for the sodium diffusion through the molybdenum and chromium layers into the forming copper indium gallium diselenide layer.

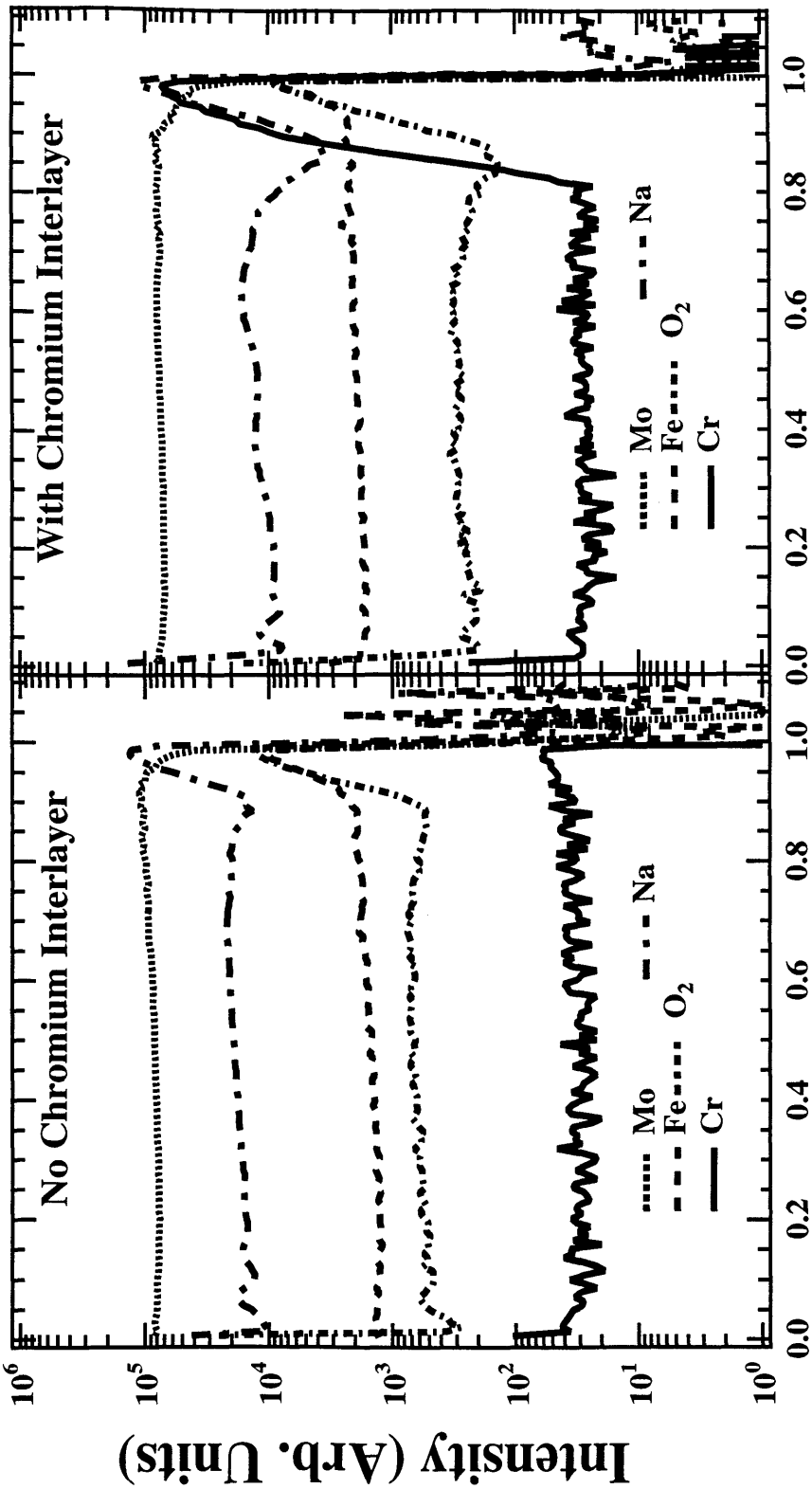

Figure 4-7. SIMS data for molybdenum films with and without a chromium interlayers show little sodium diffusion from the soda lime glass.

4.2.4 Adhesion Promotion With Glass Etching

To increase adhesion of the molybdenum to the soda lime glass, etching the surface prior to deposition was investigated. A buffered (ammonium fluoride) hydrofluoric acid solution was chosen to be the etchant because of the aggressive ability to etch silicon dioxide. The etching was performed during the cleaning process. The etch rate measured for the ten percent by volume solution used in this work was 61 nm per second.

The surface roughness was measured with an atomic force microscope; the results are shown in Figure 4-8. The as-received polished surface is made up of many small rough scratches that etch faster than a flat surface. For etches between 0 and 60 seconds the surface smoothes out. Substrates etched for sixty seconds or longer showed increasing surface roughness, greater than the as-received polished surface. This feature occurs because the surface will become rough from non-uniform etch rates across the substrate. The non-uniform etch rates could be from defects on the surface and in the bulk.

Soda lime glass substrates for later CIGS deposition were prepared by etching from forty five seconds to seventy five seconds. The longer periods of etching were chosen because of the increase in surface roughness as shown in Figure 4-8. On the majority of the substrates, foggy areas were noticed. These patches were concentrated on the tin side of the glass. These foggy areas were thought to be regions of increased surface roughness which are able to scatter light better than the surrounding

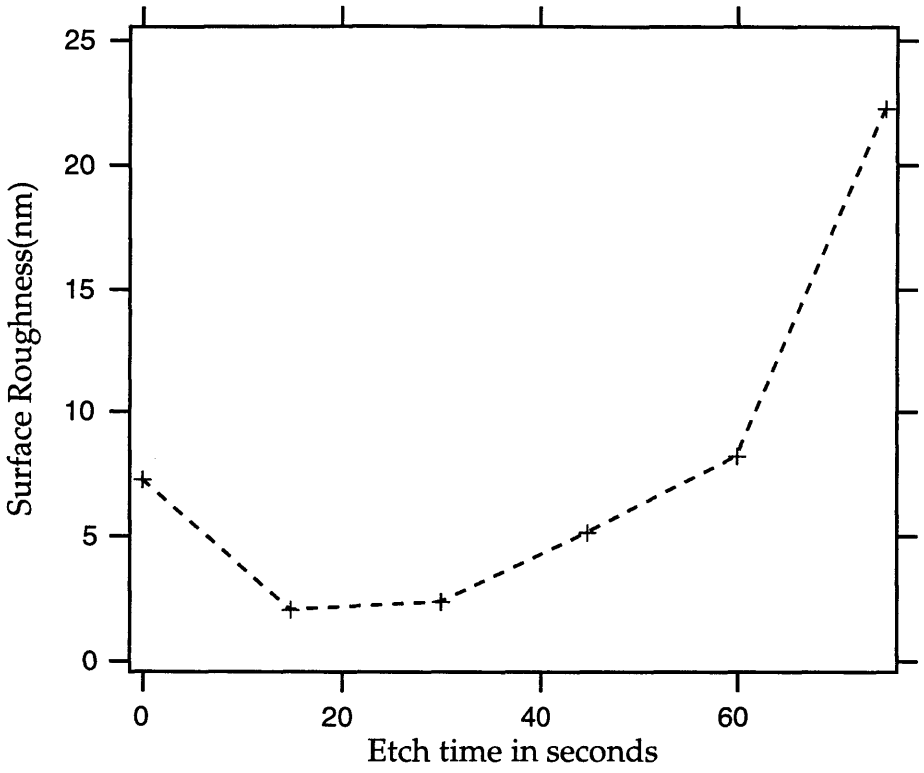

Figure 4-8. AFM median surface roughness of soda lime glass after etch.

surfaces. The substrates with the longest etch time had the highest concentration of foggy areas. Molybdenum was deposited on the air side of the soda lime glass with a sputter power of 750 Watts at 4 mTorr of pressure, sputter parameters were obtained in the first adhesion section. The adhesion of the molybdenum to the etched soda lime glass substrate was tested using the tape test and passed. A comparison of the adhesion for the etched surface and the as-received surface of the soda lime glass substrates after copper indium gallium diselenide deposition showed no real difference between adhesion and device efficiency.

4.2.5 Conclusion On Adhesion Promotion

The optimization of the sputter parameters showed that films had better adherence for 13.5-5 mTorr of pressure and higher power. A standard deposition for a 1 μm thick film of molybdenum was developed from had chromium interlayers of at least 2.3 nm never failed. The drawback to this approach was the detrimental effect on CIGS cell efficiencies. For stainless steel and alumina substrate materials where sodium diffusion is not a concern, chromium layers ensure adhesion of the molybdenum. Etching the soda lime glass substrates to increase the mechanical bond of the molybdenum was evaluated as an alternative to the chromium layer. The etched soda lime glass substrates did not show any improvement as compared to soda lime glass substrates that had not been etched. The etching only resulted in an extra process step during the cleaning of the substrates.

4.3 Oxygen Addition To Molybdenum

Oxygen impurities (O_2/Ar 0.01%) have been recently shown to promote sodium diffusion along the grain boundaries during the CIGS deposition[57]. The amount of molybdenum oxide that forms is a function of the partial pressure from residual gas evolved from the chamber walls and moisture that is in the vacuum system. The oxygen can affect the sheet resistance of the molybdenum and the maximum amount of sheet resistance ρ_s desired is 0.5 ohm to minimize power loss in the cell. Thus, there is a balance between increasing the oxygen to enhance sodium transport and maintaining a highly conductive film. For the one micron thick molybdenum film the conductivity would be 500 μOhms-cm

The molybdenum layer was deposited at 4 mTorr and 750 Watts. The flow of oxygen was set and then the argon flow increased until a system pressure of 4 mTorr was reached. Table 4-9 shows the flows of oxygen and argon added during sputtering. The sheet resistance increased with increasing oxygen flow. The sputter voltage also rose with the increased concentration of oxygen as expected. The potential between the DC magnetron and chamber walls or sputter voltage fluctuates depending on the background pressure of the chamber. The lower the background pressure the less the sputter voltage. With a minimal back ground pressure of 8×10^{-7} Torr, the sputter voltage of 310 to 320 volts is normal. The baseline sheet resistance for the standard one micron thick molybdenum film is 0.1 ± 0.02 ohms per square. The increase seen in sheet resistance, shown in Table 4-9 has been seen by others[79].

Table 4-9. Oxygen addition during molybdenum sputtering. The sputter conditions were 750 Watts of power and 4 mTorr pressure.

Sample	O_2 (sccm)	Ar (sccm)	Sputter Voltage	ρ_s ($\Omega/\square$)	Adhesion Tape Test
Control	0	9.9	318	0.12	pass
A	0.5	9.4	337	0.154-0.190	pass
B	1	9.1	338	0.156-0.239	pass
C	1.5	9.5	unknown	0.174-0.231	pass
D	2	9.9	346	0.174-0.246	pass

4.3.1 Device Performance

All samples started to peel after the copper indium gallium diselenide deposition and the samples were removed from vacuum. The failure mechanism of the film buckling was consistent with compressive stress in the film. The sample with 0.5 sccm of oxygen exhibited minor film peeling and it was possible to complete the device processing. The 0.5 sccm sample was characterized and the results are shown in Table 4-10. The device efficiency was 15.2 percent, which is typical for the baseline deposition process. The other samples were not processed into devices because of extensive peeling. The device processing was completed on the partially peeled CIGS samples six months later, the films had degraded from atmospheric exposure. Thus the efficiency results of devices 1,1.5, and 2 sccm are not representative of the performance for CIGS cells that could have been achieved had the finishing steps occurred when the absorber layers were first deposited. The results of the finished devices are shown in Table 4-10.

Table 4-10. Efficiency of CIGS Cells with oxygen added during molybdenum deposition.

Sample	V_{oc} (Volts)	I_{sc} (ma/cm^2)	Efficiency %	Fill Factor %
Control	0.6722	14.69	17.6	77
A	0.643	13.24	15.2	77
B	0	0	0	0
C	0.575	9.36	3.868	31.04
D	0.532	12.742	9.42	59.7

4.3.2 Sodium Diffusion

Intact regions of the four samples with the added oxygen and a control substrate were analyzed by SIMS. All the samples went through absorber layer processing and then were analyzed. The films with oxygen experienced peeling from a localized area to three quarters of the substrate area. The peeling occurred after deposition and does not affect the SIMS profile other than the soda lime glass interface may not be seen.

The elemental SIMS analysis of the control sample is shown in Figure 4-9. It profiles down through the copper indium gallium diselenide layer and then into the molybdenum layer. The depth scale has not been corrected for the differences in the sputter rates for copper indium gallium diselenide and molybdenum films. The copper indium gallium diselenide is actually twice as thick as shown. First note the oxygen trace, at the soda lime glass interface and at the molybdenum/CIGS interface the oxygen levels are high due to the porous growth of the off-angle sputtered molybdenum as depicted in Figure 4-4. The center of the molybdenum film has low oxygen incorporation. This low value is a result of the flux of energetic particles to backsputter oxygen from the growing molybdenum film. The profile of the oxygen in the molybdenum resembles a "V". For film not deposited under such energetic conditions the oxygen profile is flat as shown in Figure for the film with the chromium interlayer. The oxygen level in the copper indium gallium diselenide layer is low and this will be discussed later. In the molybdenum layer sodium, indium, and gallium follow the profile of the oxygen. The diffusion of indium and gallium into the molybdenum layer is along the grain boundaries. The selenium profile suggests that selenium does diffuse into the top of the molybdenum layer but not significantly along the

grain boundaries. The copper line through the molybdenum is an artifact of the analysis. Two molybdenum isotopes combine and register the same mass as the copper and the cesium mass was that was chosen for analysis.

The SIMS analysis of the four samples with added oxygen during the molybdenum deposition are shown in Figure 4-10 to Figure 4-13. The sodium and oxygen profiles through the molybdenum also show a "V" profile as seen in the control sample. Figure 4-15 shows all the oxygen traces together. The oxygen level in the molybdenum layer increases with the greater partial pressure of oxygen during sputtering. The sodium levels are shown in Figure 4-14. The sodium levels increase with the oxygen content in the molybdenum film. In the interface between the copper indium gallium diselenide and molybdenum the sodium level is the same for all samples. The amount of sodium diffusing through the copper indium gallium diselenide does not appear to be affected strongly by the source concentration at the molybdenum/CIGS interface. Unfortunately, there is no way to measure the sodium kinetics accurately in a static experiment. The indium and gallium levels also follow the increasing oxygen levels. The impurity based diffusion mechanisms for indium and gallium are like sodium but slower.

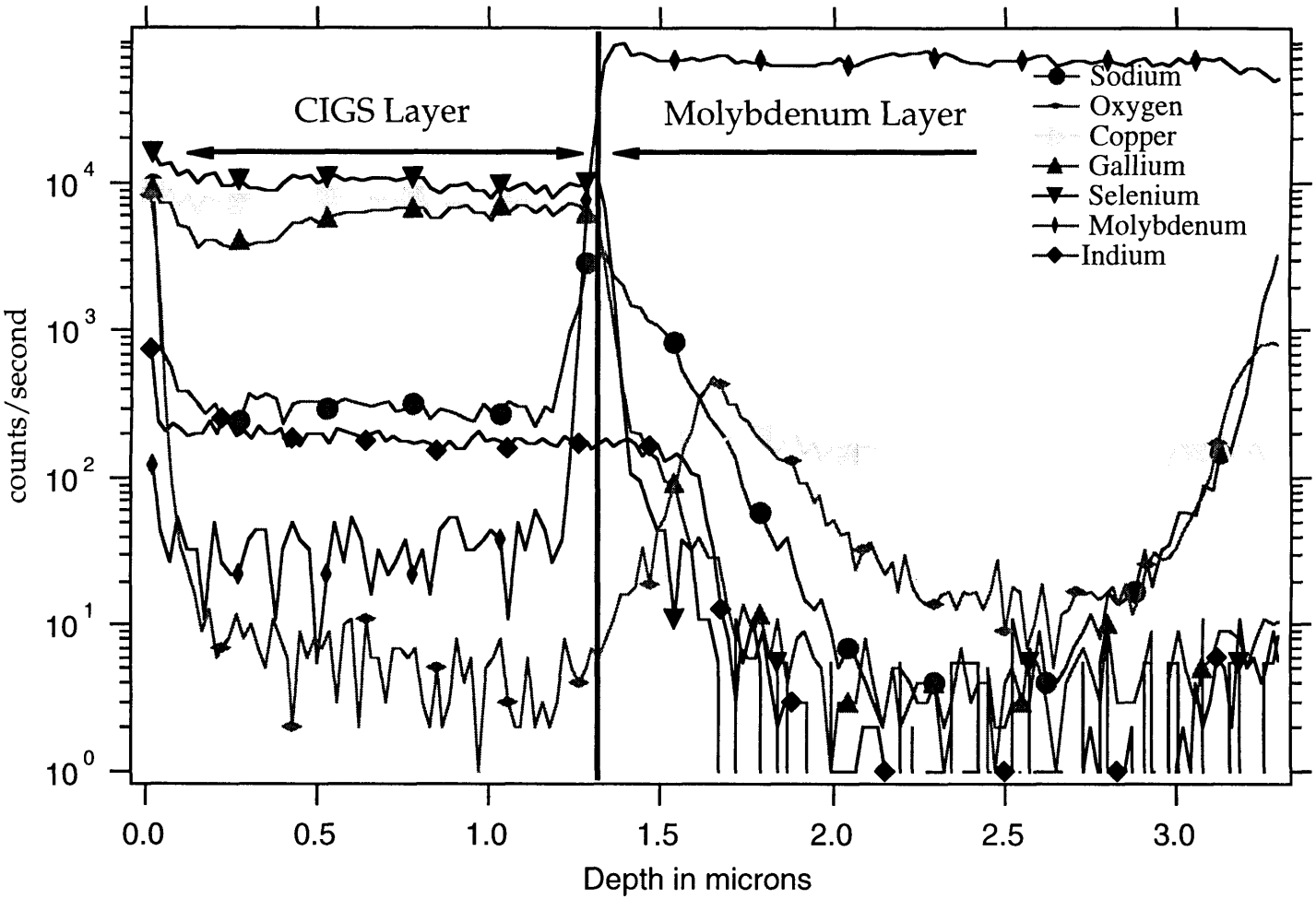

Figure 4-9. Elemental SIMS analysis of control sample without added oxygen.

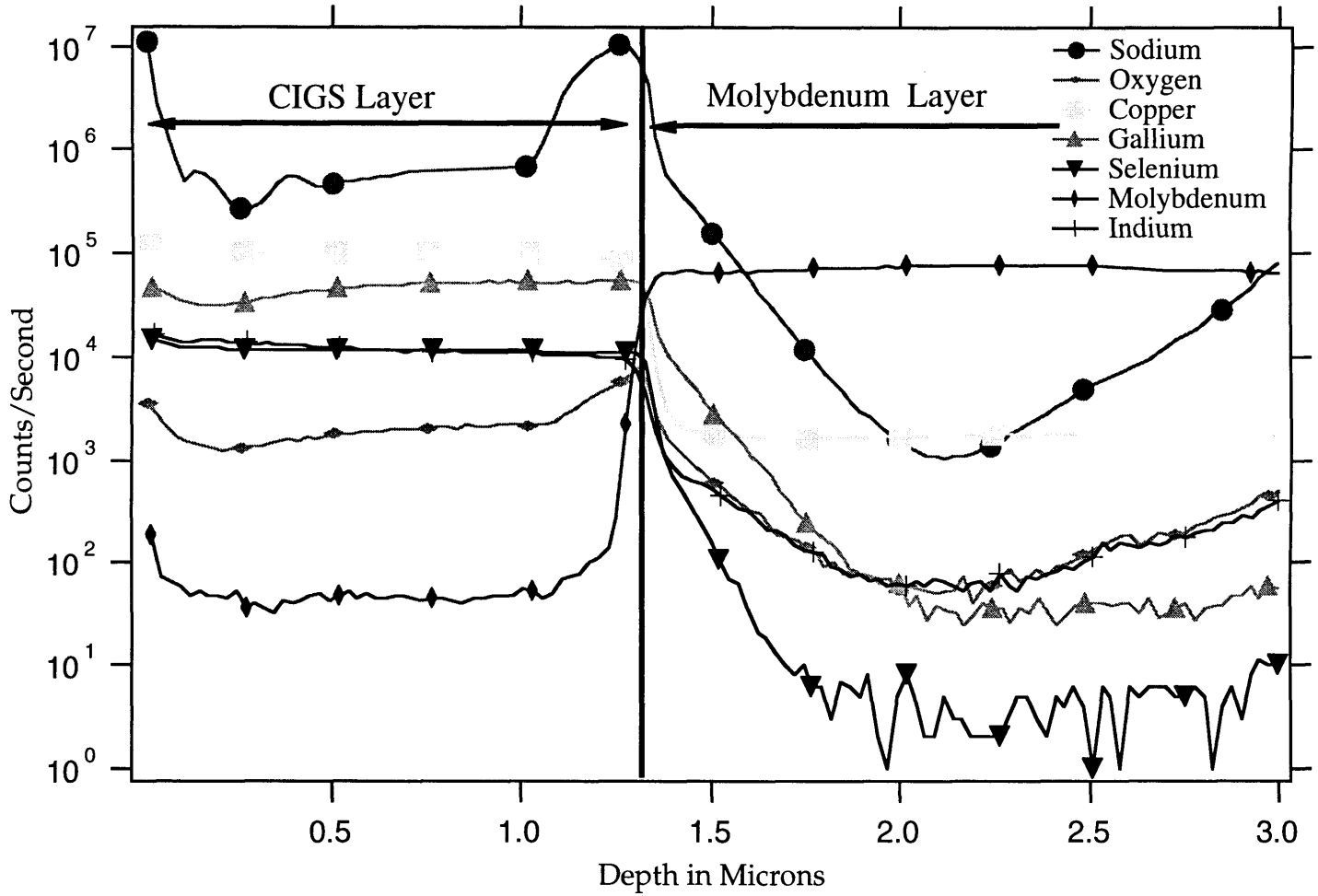

Figure 4-10. Elemental SIMS analysis of the CIGS sample with 0.5 sccm oxygen added during sputtering of the molybdenum layer.

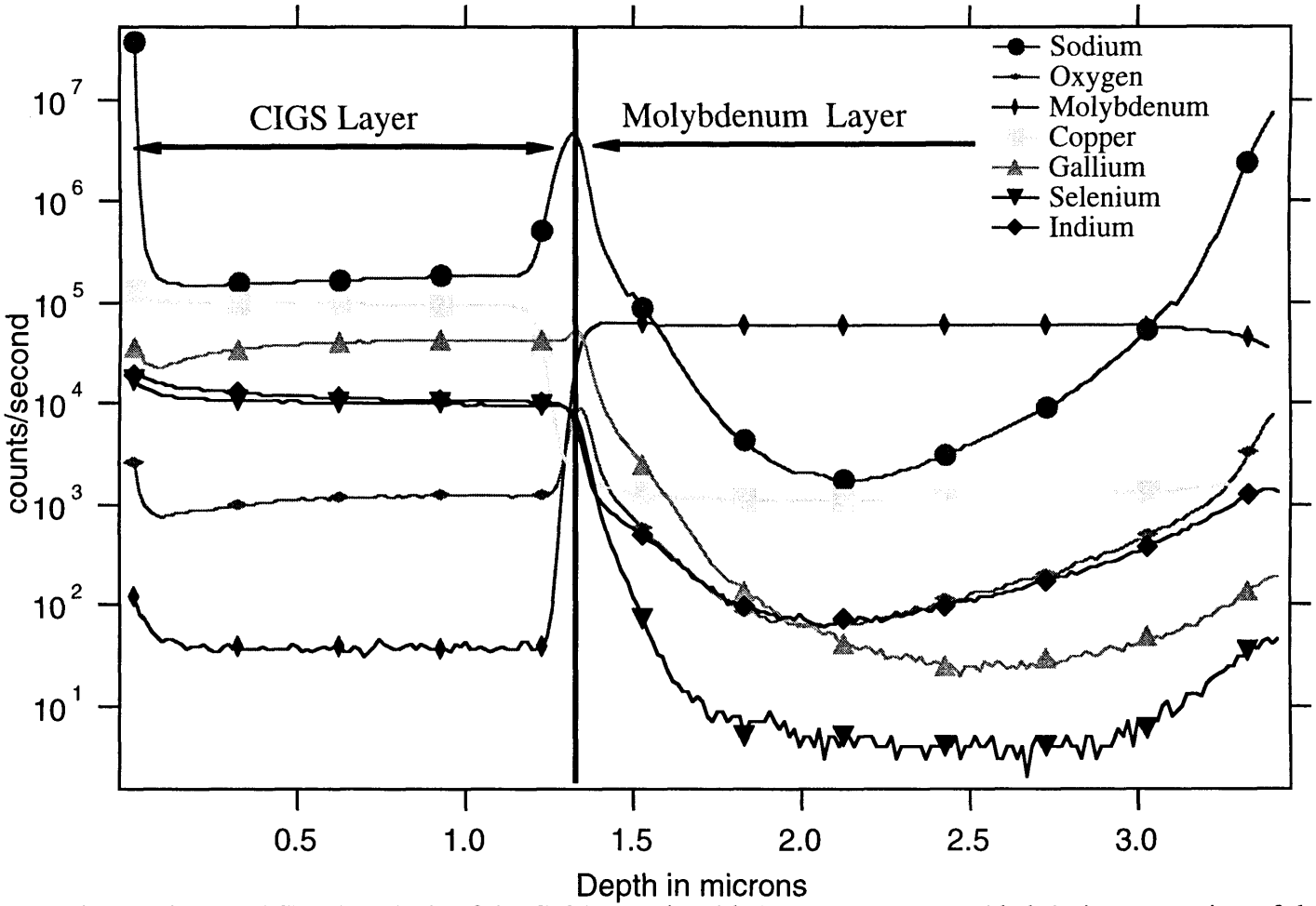

Figure 4-11. Elemental SIMS analysis of the CIGS sample with 1.0 sccm oxygen added during sputtering of the molybdenum layer.

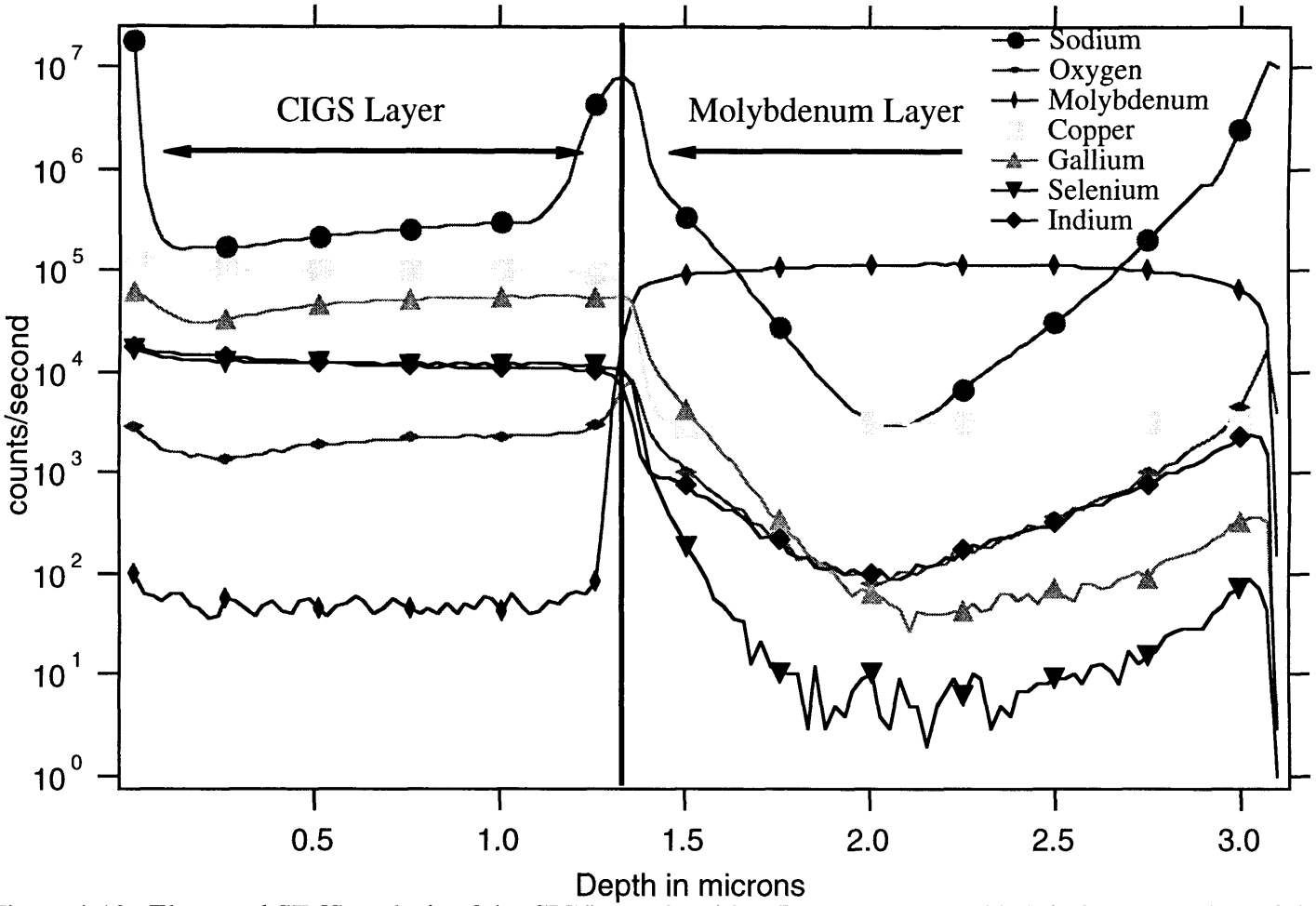

Figure 4-12. Elemental SIMS analysis of the CIGS sample with 1.5 sccm oxygen added during sputtering of the molybdenum layer.

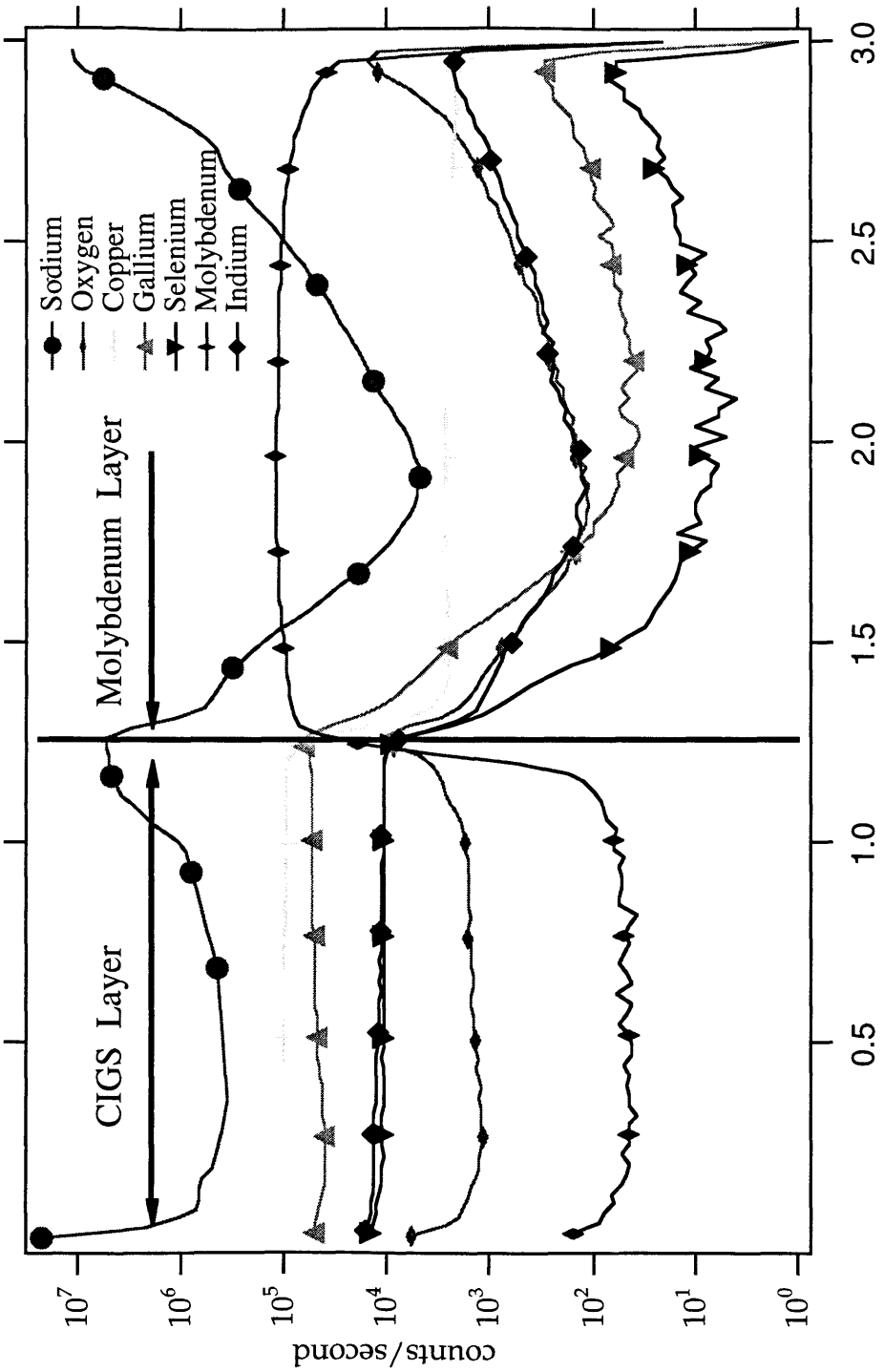

Figure 4-13. Elemental SIMS analysis of the CIGS sample with 2.0 sccm oxygen added during sputtering of the molybdenum layer.

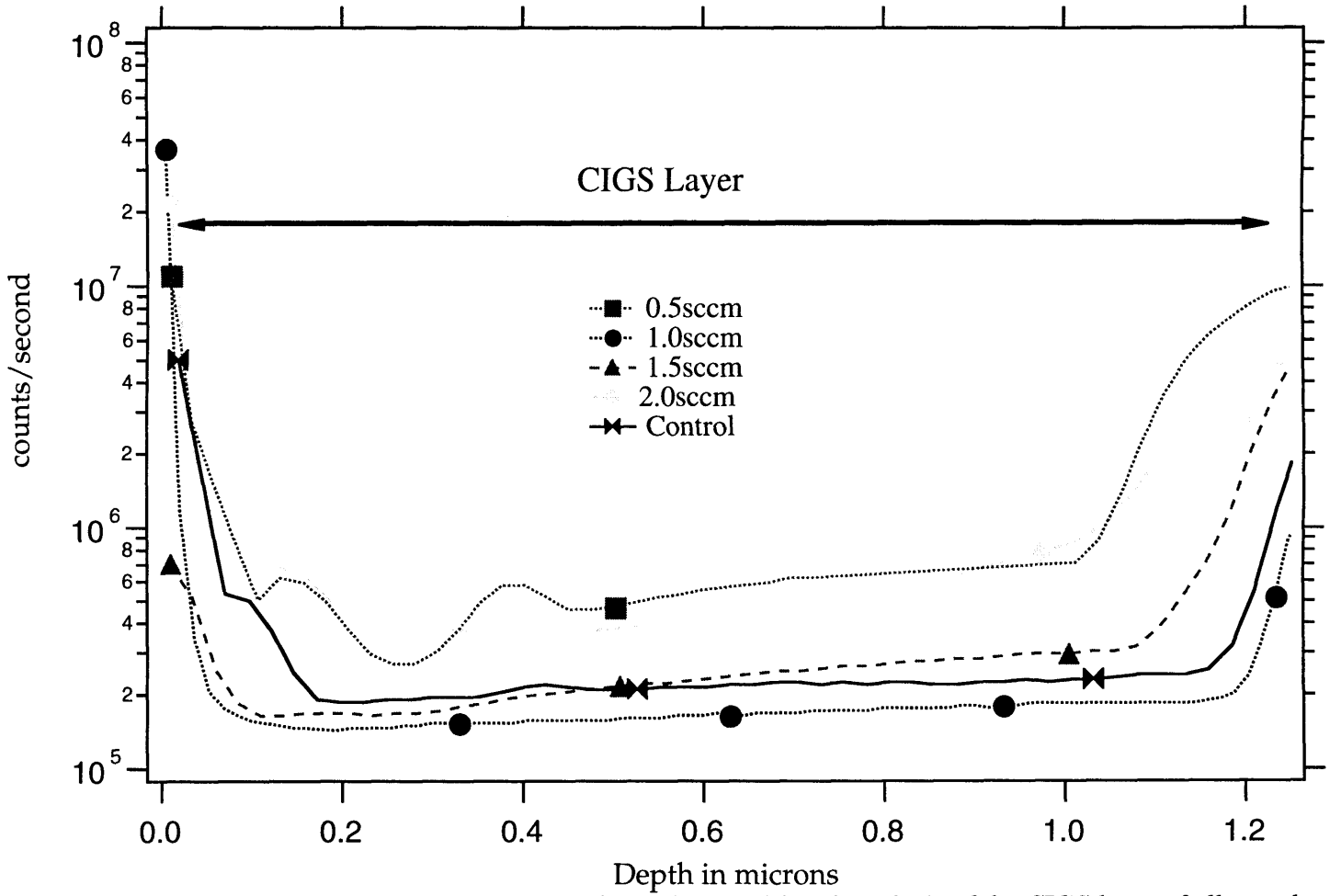

Figure 4-14. A comparison of the sodium levels from elemental SIMS analysis of the CIGS layer of all samples.

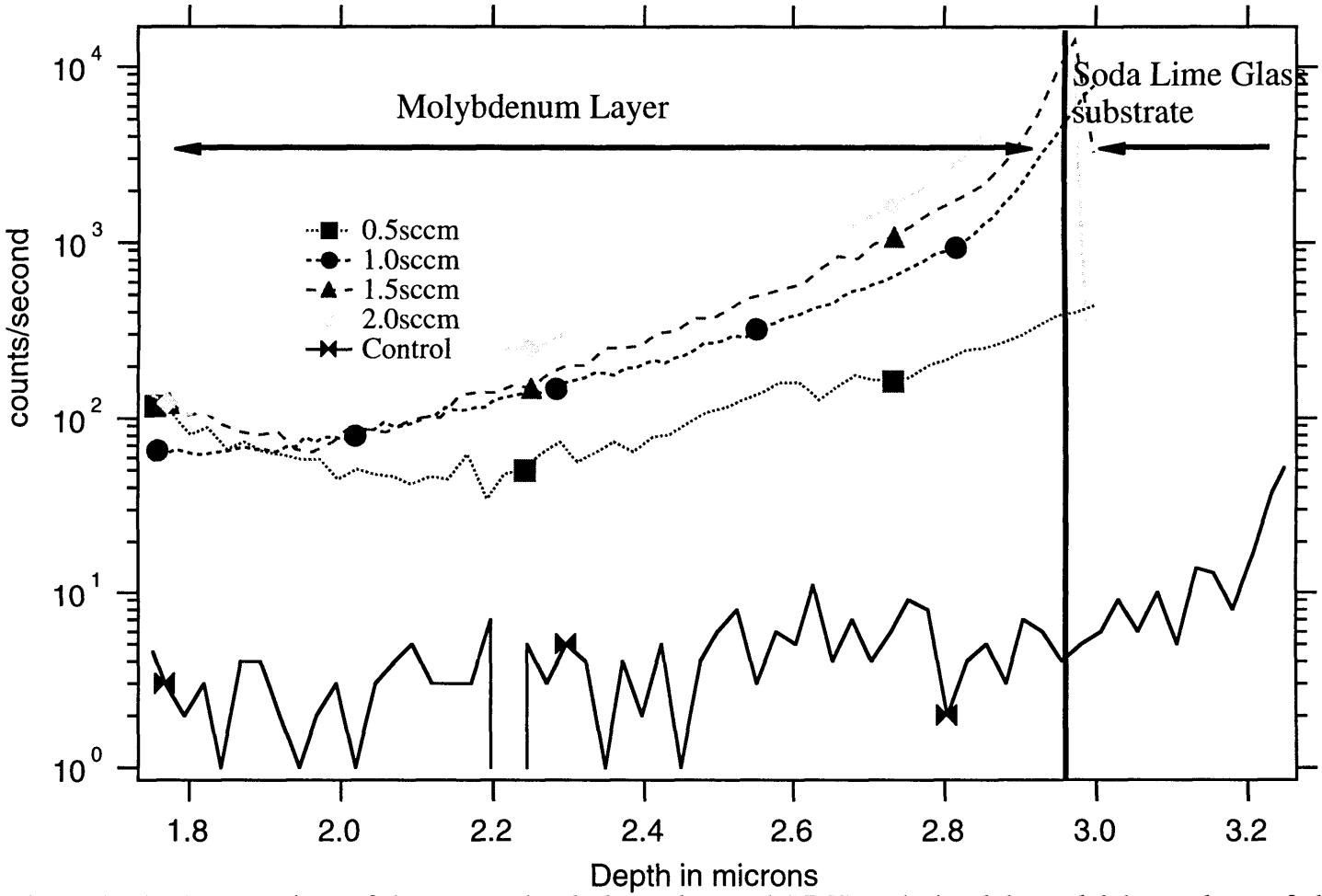

Figure 4-15. A comparison of the oxygen levels from elemental SIMS analysis of the molybdenum layer of all samples.

4.4 Characterization By X-ray Diffraction

All molybdenum films were analyzed with the following x-ray diffraction techniques: $\theta/2\theta$, pole figure, d Vs $\sin^2\Psi$.

4.4.1 $\theta/2\theta$ Measurement

The $\theta/2\theta$ measurements, with θ being the Bragg angle, showed diffraction peaks for the following orientations: 110, 200, 211, 220, 310, 222 and 321. The columnar growth of the film has sufficient order to diffract together to form the x-ray peaks. The peaks are broadened from the diffraction of the columns and consequently are not as sharply defined as a single crystal diffraction spectra. The samples showed no signs of molybdenum oxide formation. The molybdenum oxide that forms on the surface of the grain boundaries is likely randomly orientated and extremely thin giving only weak reflections that are drowned out in the background noise of the diffractometer. Figure 4-16 shows $\theta/2\theta$ measurements for the samples with oxygen and the control sample. The addition of oxygen has the effect of lowering the crystallinity of the molybdenum film. In Figure 4-17 <321> peak intensity decreases as oxygen is added during sputtering. The decreasing peak intensity is prevalent in the strong <110> peak as shown in Figure 4-18.

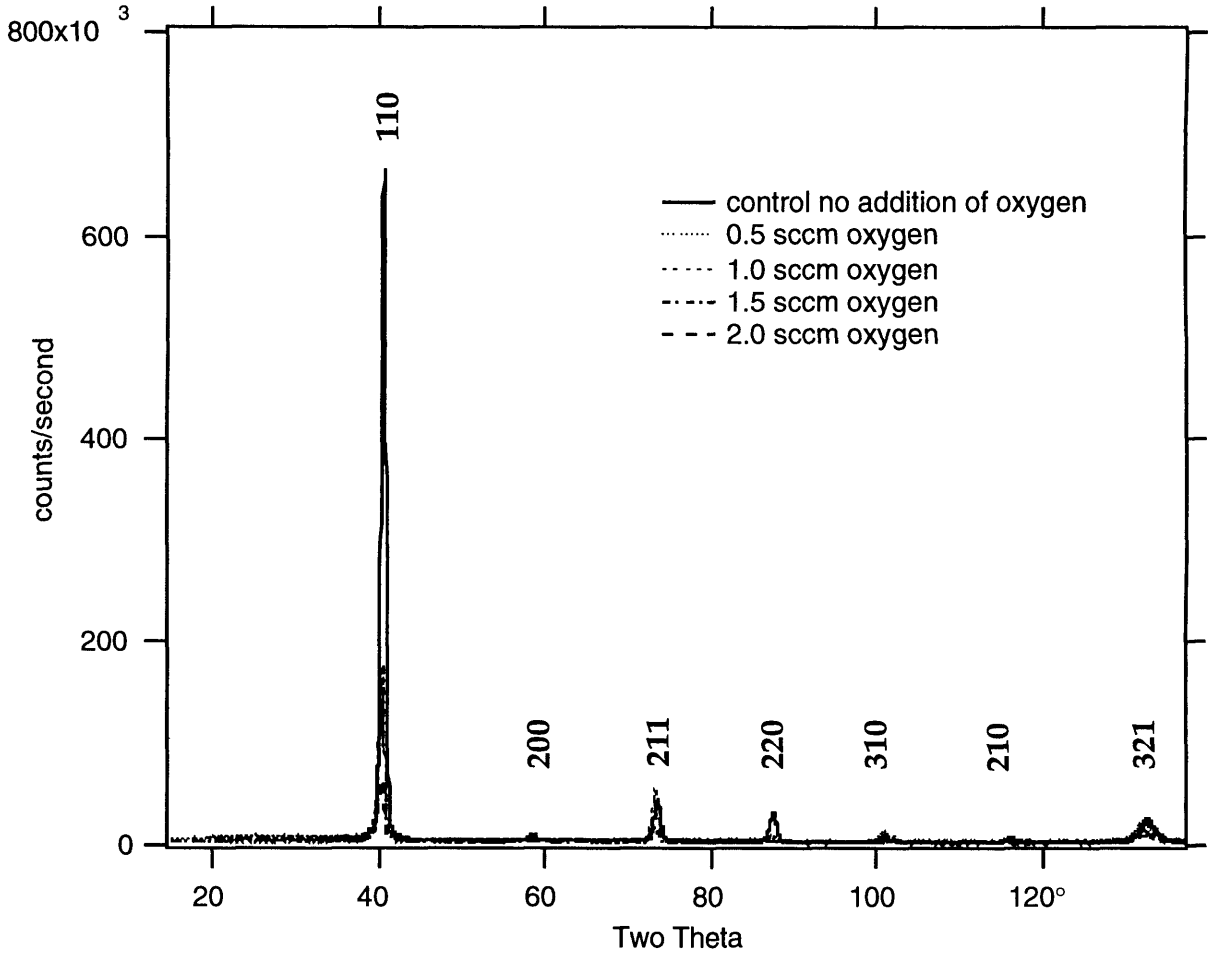

Figure 4-16. X-ray diffraction θ/2θ peak measurement of the control and samples with oxygen intentionally added during deposition of the molybdenum.

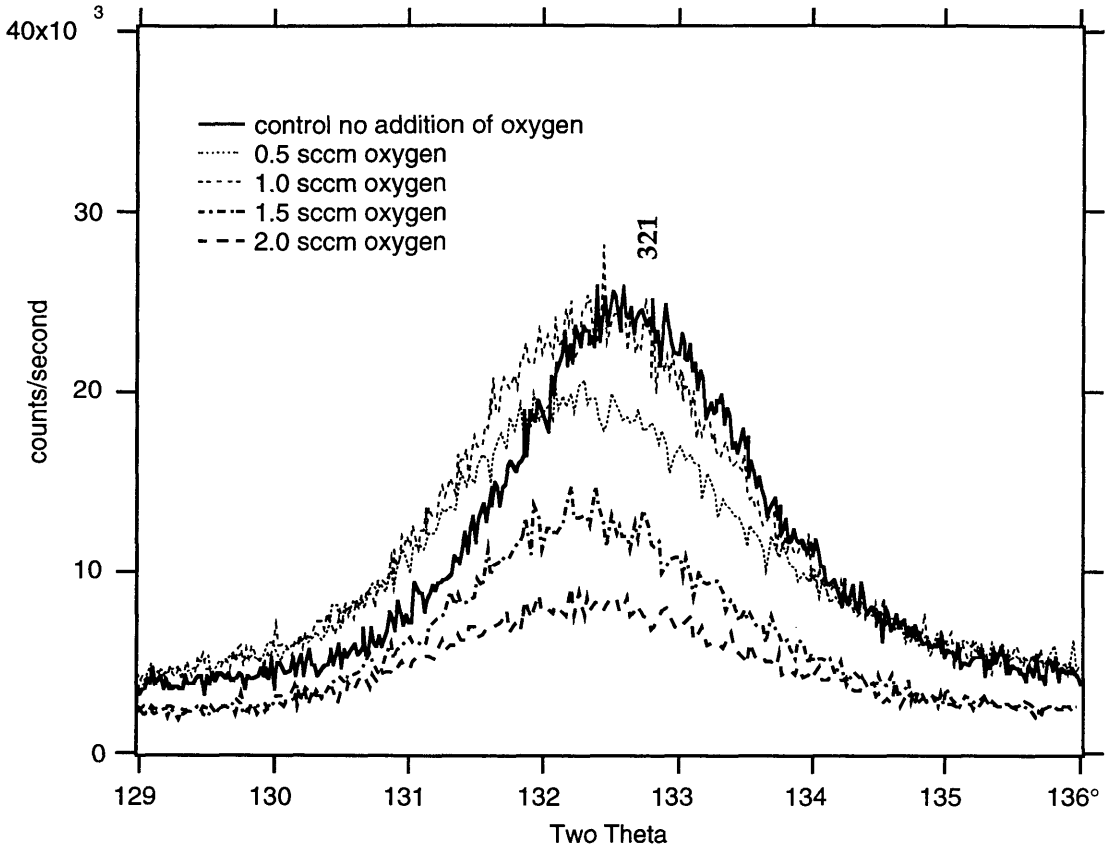

Figure 4-17. <321> X-ray diffraction θ/2θ peak showing decrease in peak intensity as a function of oxygen content.

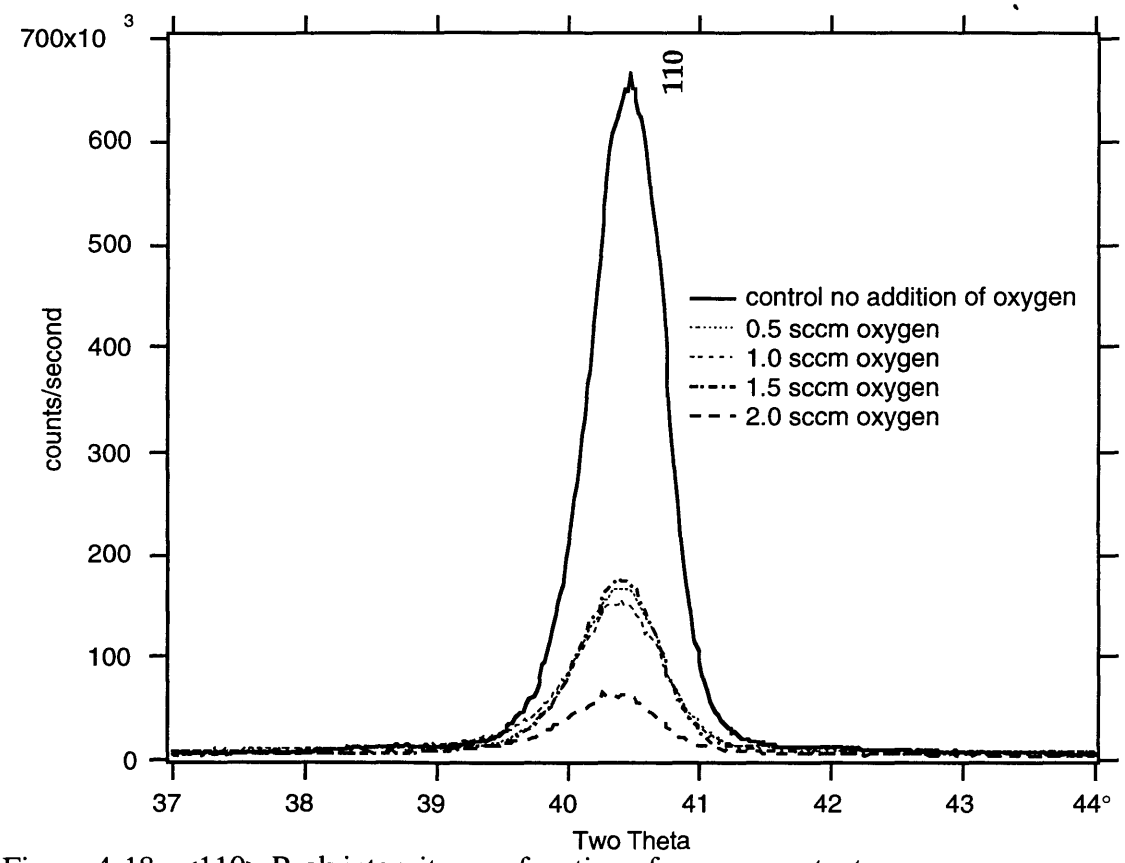

Figure 4-18. <110> Peak intensity as a function of oxygen content.

4.4.2 Texture Measurement

The pole figure measurement reflects the texture of the film. The columnar growth of the molybdenum film has a general orientation. The preferred orientation of the molybdenum is (110) normal to the surface of the substrate. The 2.0 sample sccm pole figure is shown in Figure 4-19. The samples with oxygen exhibit a different orientation as compared to the sample without oxygen in Figure 4-20.

The texture is made complex by the translation of the substrate past the DC magnetron. Analysis of the pole figures is difficult for the two examples given. The only conclusion that can be made is the oxygen influences the orientation of the molybdenum during deposition.

4.4.3 Residual Stress Measurement

The residual stress is made up of extrinsic and intrinsic forces[69]. The extrinsic forces are external forces like that generated by differences in the coefficient of thermal expansion between layers. The extrinsic stress is negligible in comparison to the intrinsic stress of the molybdenum film. The intrinsic stresses or strains are what form during the sputtering process. The factors influencing the intrinsic stress are sputter pressure, impurities, geometry, discharge voltage and temperature. The d Vs $\sin^2\Psi$ x-ray diffraction technique was used to measure residual stress in all of the molybdenum films[68]. All the films were deposited with the same sputter conditions of chamber pressure and sputter power,

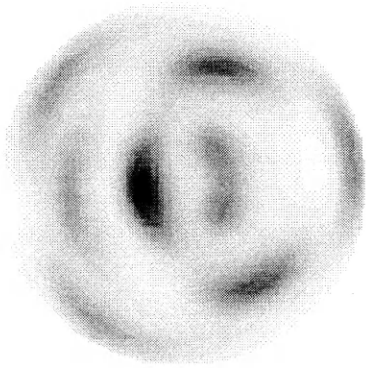

Molybdenum <110>
2.0 sccm oxygen

Figure 4-19. Pole figure for the molybdenum film with 2.0 sccm oxygen added, the dark areas represent reflection at peak intensity.

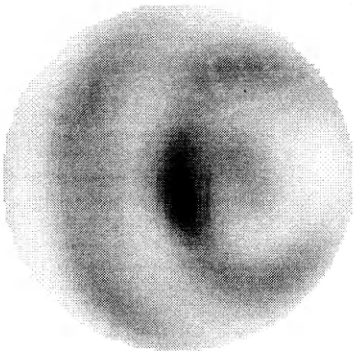

Molybdenum <110>

Figure 4-20. Pole figure for the molybdenum sample without oxygen, the dark areas represent reflection at peak intensity.

so the differences in these films were the addition of oxygen and the sputter voltage. The measurements were made on the as-deposited molybdenum films before copper indium gallium diselenide layer deposition. Table 4-11 lists the results of the residual stress measurements. The films are assumed to have biaxial stress in the plane of the film. The residual stress was measured parallel and perpendicular to the axis of translation. The results show there is a difference between the two directions. Differences in biaxial stress have been previously measured by in molybdenum films[64].

The results show that oxygen incorporation changes the films which are normally under tensile stress to compressive stress. Figure 4-21 shows a plot of the sample stress for the two in-plane measurement directions. Compressive stress is observed parallel to the translation direction and increases as the oxygen concentration increases, while the stress perpendicular to translation remains constant. The sputter voltage of all samples is over a narrow spread of 13 volts and is not responsible for the changes observed. For the molybdenum film without oxygen the tensile measurement agrees with data for sputtered films by Vink and Van Zon[80]. The residual stress of a thin film has been shown to have a reduction in tensile stress as the amount of oxygen increases[81]. The same result has been shown with a reduction in the pumping, resulting which would result in increased residual background oxygen partial pressure[82]. The increase depends on the size of the specific elements sputtered and the relative size of the oxide formed. The decrease in tensile stress is from two possible paths: (¡) grain boundary oxide formation occurs resulting in an increase in volume over the metal alone or, (¡ ¡) the energetics of the deposition are such that the resultant grain growth has spacing greater than 0.17 nm. For grain growth of

Table 4-11. In-plane residual stress measurements for the molybdenum films as a function of oxygen partial pressure.

Sample	In-plane stress perpendicular to translation (Mpa)	In-plane stress parallel to translation (MPa)	Sputter Voltage (volts)
No oxygen	355.3	430.6	350
0.5 sccm O_2	-447.3	-777.6	337
1.0 sccm O_2	-423.4	-865.6	338
1.5 sccm O_2	-327.4	-810.7	unknown
2.0 sccm O_2	-407.2	-918.9	346

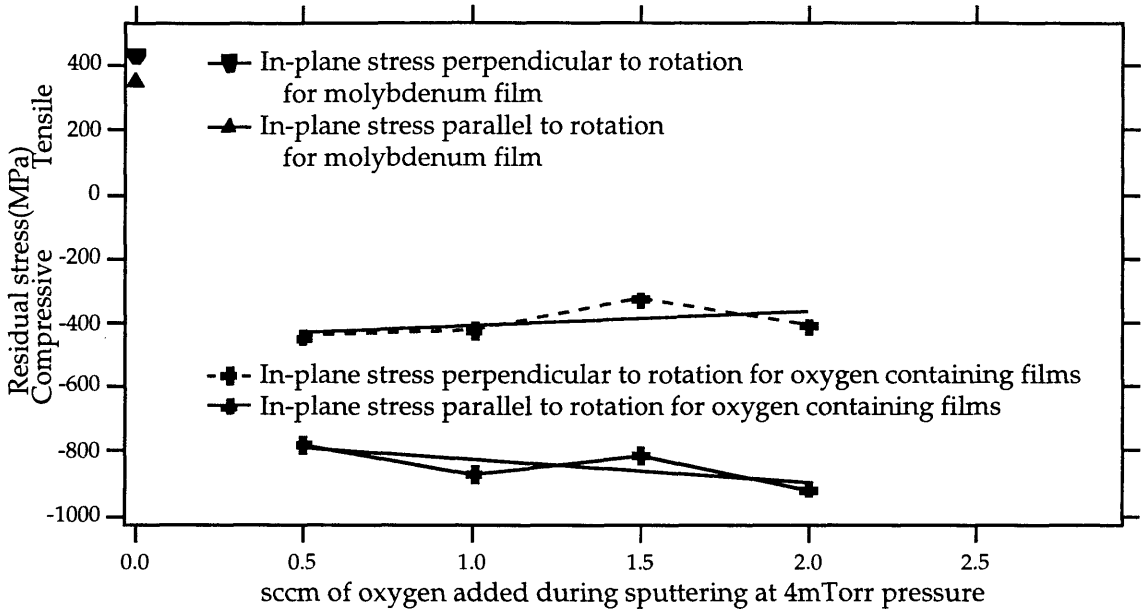

Figure 4-21. In-plane stress measurement perpendicular and parallel to the direction of substrate translation past the sputter cathode.

spacing less than 0.17 nm there is enough attractive force from the interstitial electron density increase in the metal to lead to tensile strain. The resulting residual stress is then a function of the energetics of the deposition and amount of concomitant oxygen incorporated[83].

4.4.4 Summary To The Addition Of Oxygen

The sodium content of all of the molybdenum films shows a direct correlation to the oxygen content in the molybdenum layer. The oxygen content of the molybdenum film changes as a function of position during deposition process forming a "v" profile. In the CIGS layer the sodium did not follow this trend, levels for the samples with oxygen were scattered around the control sample. The sodium content in the CIGS layer was not affected by the oxygen in molybdenum.

The addition of oxygen to the molybdenum films did not assist or improve adhesion. The sodium levels were elevated in proportion to the oxygen content of the molybdenum film. The sodium diffusion into the copper indium gallium layer was not enhanced or impeded by the additional oxygen. The efficiency for the one oxygen sample that was completed initially was in the expected device performance domain for the copper indium gallium diselenide deposition process. The addition of oxygen to the molybdenum film changed the stress from tensile to compressive and reduced the texture in the film.

4.5 Summary Of Results And Discussion

The Leybold Heraeus deposition system was employed for molybdenum deposition because of the ability to coat multiple substrates in a single deposition run. Molybdenum was sputter deposited with a DC magnetron. For much of the parameter space investigated the molybdenum films were found to have marginal adhesion characteristics on soda lime glass substrates. The adhesion of the molybdenum improved as the deposition sputter power increased. The Leybold Hereaus system imposed limits on how the deposition of molybdenum would take place. The translation of the platen was fixed and the desired thickness of one micron limited the power used to sputter the molybdenum. The sputter pressure was then found to minimize the residual stress of the molybdenum film which helped adhesion to the soda lime glass. A thin chromium layer between the molybdenum and the soda lime glass assured adhesion. The thickness for the chromium was only five to ten nanometers thick. The CIGS cell performance was found to be impaired on substrates that had a chromium adhesion layer. The same performance difference is observed in CIGS cells with limited sodium content. The cause of the lowered performance is suspected to be related to reduced sodium diffusion through the chromium layer. The effects of the sodium in CIGS cells is not fully understood. The use of the chromium adhesion layers on soda lime glass results in a trade-off between adhesion and lower CIGS cell performance. The chromium adhesion layer is applicable to other types of substrates as well. Another possible method to improve the adhesion without chromium was a surface treatment prior to molybdenum deposition. The surface of the soda lime glass was etched to enhance the surface roughness and improve the bond of the molybdenum to the soda

lime glass. The etching of the soda lime glass did not improve the adhesion of the molybdenum.

The beneficial effects of sodium diffusion from the soda lime glass on CIGS cell performance are established. The diffusion of sodium is aided by the oxygen impurities found at the grain boundaries of the molybdenum. Increased oxygen levels in the molybdenum film did not affect the sodium levels in the CIGS layer. The addition of oxygen did change the structure of the molybdenum during sputtering. X-ray diffraction revealed lower intensity peaks for the molybdenum as increased amounts of oxygen were added during sputtering. The residual stress in the molybdenum film changed from a tensile state to a compressive state resulting in reduced adhesion. Molybdenum films under compression state have previously been observed to have poor adhesion[64]. Thus, the adhesion failure found after the CIGS layer was deposited was not an unexpected result.

5. CONCLUSION

1. Results showed that molybdenum adheres to the soda lime glass substrate better for higher sputter power and for sputter pressures of 3-5 mTorr. No adhesion advantage was found for either side of the soda lime glass. The air side was chosen to deposit the molybdenum on because of the potentially unknown effects on the tin side from tin diffusion into the copper indium gallium diselenide layer.

2. The addition of a thin chromium interlayer insured adhesion of the molybdenum to the substrate. The CIGS cells deposited on soda lime glass substrates with a chromium interlayer consistently had lower device performance. The chromium was suspected to act as a diffusion barrier. Etching the soda lime glass increased surface roughness of glass, but did not improve adhesion of the molybdenum to the substrate.

3. The elemental SIMS analysis showed that the sodium content in the molybdenum layer followed the shape of the oxygen trace through the molybdenum layer. The sodium content of the CIGS layer was found not to be affected by the increased oxygen levels in the molybdenum. The addition of oxygen during sputtering changed the structure of the molybdenum and the residual stress. The texturing of the molybdenum film decreased as oxygen content was increased.

6. FUTURE DEVELOPMENT

The work done here was to optimize the adhesion of molybdenum films to the soda lime glass substrate with in the limits of the deposition system. Parameters for good adhesion were found but the fundamental difference between a film with good or bad adhesion was not identified. The interface between the soda lime glass and the molybdenum should be characterized and modeled. The films that exhibited good adhesion were deposited at greater sputter power conditions. A model could be developed for the molybdenum adhesion as a function of energy necessary to have pseudodiffusion at the soda lime glass surface.

The chromium layer provided excellent adhesion properties but was found to block the sodium. The use of a titanium adhesion layer in place of the chromium layer would be worth the effort to determine if the titanium forms a barrier layer. The titanium adhesion layer has been found to be a barrier layer for metal diffusion when the titanium is partially oxidized[41].

The diffusion rate of the sodium is difficult to measure. The suggested research should focus on measuring the diffusion of sodium through the molybdenum layer. The current understanding of diffusion of sodium is indirectly understood by looking at the sodium content after deposition of the CIGS layer. Through diffusion rate measurements, the

affects of grain structure, residual stress, oxygen content and film thickness could be correlated to sputter process parameters.

7. REFERENCES CITED

1. Tuttle, J.R., Ward, J.S., Duda, A., Berens, T.A., Contreras, M.A., Ramanathan, K.R., Tennant, A.L., Keane, J., Cole, E.D., Emery, K. and Noufi, R. "The Performance of Cu(In,Ga)Cu Based Solar Cells in Conventional and Concentrator Applications." In Materials Research Society Symposium, San Fransisco, CA, (1996).

2. Tuttle, J.R., Berens, T.A., Keane, J., Ramanarhan, K.R., Granada, J., Bhattacharya, R.N., Weisner, H., Contreras, M.A. and Noufi, R. "Investigations into Alternative Substrate, Absorber, and Buffer Layer Processing for Cu(In,Ga)Se_2-Based Solar Cells." In 25th IEEE PVSC, Washington, DC, (1996).

3. Ruckh, M., Schmid, D., Kiaser, M., Schaffler, R., Walter, T. and Schock, H.W. "Influence of Substrates on The Electrical Propetries of Cu(In,Ga)Se_2 Thin Films." In 1st World Conference on Photovoltaic Energy Conversion, Waikoloa, Hawaii, IEEE, New York, 156, (1994).

4. Granata, J.E., Sites, J.R., Asher, S. and Matson, R.J. "Quantative Incorporation of Sodium in CIS and CIGS Photovoltaic Devices." In 26th IEEE PVSC, Anaheim, CA, (1997).

5. Bodegard, M., Stolt, L. and Hedstrom, J. "The Influence of Sodium on the Grain Structure of $CuInSe_2$ Films for Photovoltaic Applications." In 12th European Photovoltaic Solar Energy Conference, Amsterdam, The Netherlands, H. S. Stephens & Associates, Felmersham(1994).

6. Matson, R.J., Jamjoum, O., Buonaquisti, A.D., Russell, P.E., Kazmerski, L.L., Sheldon, P. and Ahrenkiel, R.K. "Metal Contacts to $CuInSe_2$."*Solar Cells* (1984), *11*, 301-305.

7. Russell, P.E., Jamjoum, O., Ahrenkiel, R.K. and Kazmerski, L.L. "Properties of the Mo-$CuInSe_2$ Interface."*Applied Physics Letters* (1982), *40*, 995-997.

8. Gabor, A.M. The Conversion of (In, Ga)$_2$Se Thin Films to Cu(In,Ga)Se$_2$ for Application to Photovoltaic Solar Cells,PhD Thesis, University of Colorado,Boulder, CO, (1995).

9. Lindahl, K. Quantative Investigation of Copper/Indium Multilayer Thin Film Reactions,PhD Thesis, Colorado School of Mines,Golden, CO, (1996).

10. Berens, T.A. Cu(In,Ga)Se$_2$ Absorbers Fabricated from Sputtered Precursors,MS Thesis, Colorado School of Mines,Golden, CO, (1997).

11. Chu, T.L., Chu, S.S., Ferekides, C., Wu, C.Q., Britt, J. and Wang, C. "High Efficiency CdS/CdTe Solar Cells From Solution-Grown CdS Films." In Conference Record of the Twenty Second IEEE Photovoltaic Specialists Conference, Las Vegas, NV, IEEE, New York, NY, USA, 952-6, (1991).

12. Fromment, M., Bernard, M.C., Cortes, R., Mokili, B. and Lincot, D. "Study of CdS Epitaxial Films Chemically Deposited from Aqueous Solutions on InP Single Crystals."*J. Electrochemistry Soc* (1995), *142*, 2642-2649.

13. Contreras, M. Thin-Film Polycrystalline Cu-In-Ga-Se For Photovoltaic Applications,Thesis, Colorado School of Mines,Golden, CO, (1996).

14. Walter, T. and Schock, H.W. "Fundimential Studies and Development of Technologies for CuInSe$_2$ Thin Film Solar Cells in The Eurocis Program." In 12th NREL Photovoltaic Program Review, Denver, NREL(1993).

15. Probst, V., Karg, F., Rimmasch, J., Riedl, W., Stetter, W., Harms, H. and Eibl, O. "Advanced Stacked Elemental Layer Process For Cu(In,Ga)Se$_2$ Thin Film Photovoltaic Devices." In Materials Research Society Symposium, San Fransisco, CA, (1996).

16. Scofield, J.H., Asher, S., Albin, D., Tuttle, J.R., Contreras, M., Niles, D., Ready, R., Tennant, A. and Noufi, R. "Sodium Diffusion, Selenization, and Microstructural Effects Associated with Various Molybdenum Back Contact Layers For CIS-Based Solar Cells." In 1st World Conference on Photovoltaic Energy Conversion, Waikoloa, Hawaii, IEEE, New York,1993, 164, (1994).

17. Hill, R.J. *Physical Vapor Deposition*; (BOC Group: 1986);

18. Cuthrell, R.E., Mattox, D.M., Peeples, C.R., Dreike, P.L. and Lamppa, K.P. "Residual Stress Ansotropy, Stress Control, and Resistivity in Post Cathode Magnetron Sputter Deposited Molybdenum Films."*Vacuum Science and Technology A* (1988), *6*, 2914-2920.

19. Thornton, J.A. and Hoffman, D.W. "Stress Related Effects in Thin Films."*Annual Review in Material Science* (1989), 5-32.

20. Windischmann, H. "Intrinsic Stress in Sputter Deposited Thin Films."*Critical Reviews in Solid State and Material Sciences* (1992), *17*, 547-596.

21. Pulker, H.K. *Coatings on Glass*; (Elsevier: Amsterdam, 1984);

22. Penfold, A.S. "Early Days of Magnetron Sputtering -An Enigma."*Thin Solid Films* (1989), *171*, 99-108.

23. Chapman, B. *Glow Discharge Process*; (Wiley & Sons: 1980);

24. Nix, W.D. "Mechanical Propetries of Thin Films."*Metallugical Transactions A* (1989), *20A*, 2217.

25. Neugebauer, C.A. In *Handbook of Thin Film Technology*; L. I. Maissel and R. Glang, Eds.; (McGraw-Hill: New York, NY, 1968);

26. Frost, H.J. "Microstructural Evolution in Thin Films."*Materials Characterization* (1994), *32*, 257-273.

27. Grovenor, C.R.M., Hemtzell, H.T. and Smith, D.A. "The Developement of Grain Structure During Growth of Metallic Films."*Acta Metallergy* (1984), *32*, 773-781.

28. Hoffman, D.W. "Internal Stresses in Cr, Mo, Ta, and Pt Films Deposited by Sputtering from a Planar Magnetron Source."*Journal of Vacuum Science and Technology* (1982), *20*, 355-358.

29. Thornton, J.A. and Hoffmann, D.W. "The Influence ofDischarge Current on The Intrinsic Stress in Mo Films Deposited Using Cylindrical and Planar Magnetron Sources."*Journal of Vacuun Science and Technology* (1985), *A 3*, 576-579.

30. Movchan, B.A., Demchishin, A.V. and Kooluck, L.D. "Structure and Mechanical Propetries of Thick Fe, Fe-NbC, Fe-Ni-NbC Condensates."*Journal of Vacuum Science and Technology* (1974), *11*, 869.

31. Thornton, J.A. "High Rate Thick Film Growth."*Annual Material Science Review* (1977), 239-260.

32. Muller, K.H. "Dependance of Thin Film Microstructure on Deposition by Rate Means of Computer Simulation."*Journal of Applied Physics* (1985), *58*, 2573.

33. Ramanlal, P. and Sander, L.M. "Theory of Ballistic Aggregation."*Physical Review Letters* (1985), *54*, 1828-1831.

34. Dirks, A.G. and Leamy, H.J. "Microstructure and Magnetism in Amorphos Rare-Earth-Transition-Metal Thin Films. I. Microstructure."*Journal of Applied Physics* (1978), *49*, 3430.

35. Kim, S. and Henderson, D.J. "Computer Simulation of Amorphous Thin Films of Hard Spheres."*Thin Solid Films* (1977), *47*, 155.

36. Balluffi, R. and Blakely, J.M. "Special Aspects of Diffusion."*Thin Solid Films* (1975), 363.

37. Shewmon, P.G. *Diffusion in Solids*; (The Minerials, Metals and Materials Society: Warrendale, PA, 1989);

38. Tu, K.N. "Interdiffusion in Thin Films."*Annual Review in Materials Science* (1985), *15*, 147-76.

39. DuMond, J.W.M. and Youtz, J.P. "Selective X-ray Diffraction From Artifically Stratified Metal Films Deposited by Evaporation."*Physical Review* (1935), *48*, 703.

40. DuMond, J.W.M. and Youtz, J.P. "An X-ray Method of Determining Rates of Diffusion in The Solid State."*Journal of Applied Physics* (1940), *11*, 357.

41. Nicolet, M.A. "Diffusion Barriers in Thin Films."*Thin Solid Films* (1978), 415-443.

42. Fournier, P.R.,Gate Metallization Structure USA 3,879,746 , 1975.

43. Totta, P.A. and Sopher, R.P. *IBM Journal of Research Devices* (1969), 225.

44. Harris, J.M., Lugujjo, E., Campisano, S.U., Nicolet, M.A. and Shima, R. "Studies on The Al203-Ti-Mo-Au Metalization System."*Journal of Vacuum Science and Technology* (1975),

45. Zhang, S.B., Wei, S.H. and Zunger, A. "Defect Physics of The CIS Chalcopyrite Semiconductor."*Physics Review Letters* (1997), *78*, 4059-4062.

46. Neumann, H. "Optical Propetries and Electronic Band Structure of $CuInSe_2$."*Solar Cells* (1986), *16*, 317-333.

47. Olson, D.L. and Edwards, G.R. "Interfacially Driven Mass Transport in Joining and Coating Technologies."*Philosophical Transactions* (1997),

48. Mullins, W.W. "Two Dimensional Motion of Idealized Grain Boundaries."*Journal of Applied Physics* (1956), *27*, 900-904.

49. Thompson, C.V. and Smith, H.I. "Surface-Energy-Driven Secondary Grain Growth in Ultrathin (<100 nm) Films of Silicon."*Applide Physics Letters* (1984), 603-605.

50. Thompson, C.V. "Secondary Grain Growth in Thin Films of Semiconductors: Theoretical Aspects."*Journal of Applied Physics* (1985), *52*, 763-772.

51. Frost, H.J. and Thomson, C.V. "Computer Simulation of Microstructural Evolution in Thin Films."*Journal of Electronic Materials* (1988), *17*, 447-458.

52. Hillert, M. "On The Theory of Normal and Abnormal Grain Growth."*Acta. Metall.* (1965), *13*, 227-238.

53. Rollett, A.D., Srolovitz, D.J. and Anderson, M.P. "Computer Simulation of Grain Growth- V. Abnormal Grain Growth."*Acta. Metall.* (1985), *33*, 2233-2247.

54. Julien, C., El-Farh, L. and Balkanski, M. "The Growth and Electrochemical Propetries of Metal-Oxide Thin Films."*Applied Surface Science* (1993), 325-330.

55. Granqvist, C.G. *Handbook of Inorganic Electrochromic Materials*; (Elsevier Science: Amsterdam, 1995);

56. Bodegard, M., Hedstrom, J., Ganath, K., Rockett, A. and Stolt, L. "Na Precursors For Coevaporated $Cu(In,Ga)Se_2$ Photovoltaic Films." In (1995).

57. Granath, K., Stolt, L., Bodegard, M., Rockett, A. and Schroeder, D.J. "Sodium in Sputtered Mo Back Contacts For $Cu(In,Ga)Se_2$ Devices: Incorporation, Diffusion, and Relationship To Oxygen." In 14th Euorpean Photovoltaic Solar Energy Conference, Barcelona Spain, (1997).

58. Rothenburg, G.B. *Glass Technology, Recient Developements*; (Noyes Data Corporation: Park Ridge, NJ, 1976);

59. Goodyear, J.K. and Lindberg, V.L. "Low Adsorption Float Glass for Back Surface Solar Reflectors."*Solar Energy Materials* (1980), *3*, 57.

60. Pitts, J.R. "Silver-Silicon Bonding on Silica Surfaces," Solar Energy Research Institute, (1985).

61. Doremus, R.H. *Glass Science*; (Academic Press: New York, 1973);

62. Daniel, J.L. and Coleman, J.E. "Progressive Changes in Microstructural and Composition During Degradation of Solar Mirrors."*Solar Energy Materials* (1980), *3*, 135-150.

63. Hieber, K. and Lassak, L. "Structural and Electrical Propetries of Chromium and Nickel Films Evaporated in The Presence of Oxygen."*Thin Solid Films* (1974), *20*, 63-773.

64. Scofield, J., Duda, A., Albin, D., Ballard, B.L. and Perdecki, P.K. "Effects of Argon Pressure on the Properties of Sputtered Molybdenum Films for CIS and CIGS Thin Film Solar Cell Back Contact Appliations." In 1st World Conference on Photovoltaic Energy Conversion, Waikoloa, Hawaii, IEEE,New York(1994).

65. ASTM "Test method for sheet resistance of thin metalic films with a collinear four point probe," American Standard Testing and Materials, (1978).

66. Cullity, D.B. *Elements of X-ray Diffraction*; (Addison-Wesley: Reading, Massachusetts, 1967);

67. Ballard, B.L., Predecki, P.K. and Braski, D.N. "Stress Depth Profiles in Magnetron Sputtered Mo films Using Grazing Incidence X-ray Diffraction."*Advances in X-ray Analysis* (1994), *37*, 189.

68. Clemens, B.M. and Bains, J.A. "Sress Determination in Textured Thin Films Using X-ray Diffraction."*Materials Research Society bulletin* (1992), 46-51.

69. Noyan, I.C. and Cohen, J.B. *Residual Stress Measurement by Diffraction and Interpretation*; (Springer-Verlag: New York, 1987);

70. Noyan, I.C., Huang, T.C. and York, B.R. "Residual Stress/Strain Analysis in Thin Films by X-ray Diffraction."*Critical Reviews in Solid State Materials* (1995), *20*, 125-177.

71. Tuttle, J.R., Contreras, M., Tenneant, A., Albin, D. and Noufi, R. "High Efficiency Thin Film Cu(In,Ga)Se_2 Base Photovoltaic Devices: Progress Tward a Universal Approach to Absorber Fabrication." In 24 th IEEE Photovoltaics Specialist Conference, , 415, (1993).

72. Hauffe, K. *Oxidation of Metals*; (Plenum Press: New York, 1965);

73. Birks, N. and Meier, G.H. *Introduction To High Temperature Oxidation of Metals*; (Edward Arnold: 1983);

74. Gulbransen, E.A. and Jansson, S.A. In *Oxidation of Metals and Alloys*; (American Society for Metals: Metals Park Ohio, 1970);

75. Karunasiri, R.P.U., Bruinsma, R. and Rudnick, J. "Thin-Film Growth and the Shaddow Instability."*Physical Review Letters* (1989), *62*, 788-791.

76. Muller, K.H. "Monte Carlo Calculation for Structural Modifications in Ion-Assisted Thin Film Deposition Due to Thermal Spikes."*Journal of Vacuum Science and Technology* (1986), *A4*, 184.

77. *Smithell's Metals Reference Book*; Brandes, E.A. and Brook, G.B., Eds.; Butterworth-Heinemann: Oxford, 1992; Vol. 7.

78. Granath, K., Rockett, A., Bodegard, M., Nender, C. and Stolt, L. "Mechanical Issues of Mo Back Contacts for Cu(In,Ga)Se_2 Devices." In 13th European Photovoltaic Solar Energy Conference, Nice, France, H. S. Stephens & Associates, Felmersham(1995).

79. So, F.C.T., Kolawa, E., Nieh, S.C.W., Zhao, X.A. and Nicolet, M.A. "Propetries of Reactively Sputtered $Mo_{1-x}O_x$ Films."*Applied Physics A* (1988), 265-270.

80. Vink, T.J. and Zon, J.B.A.D.v. "Stress is Sputtered Mo Thin Films: The Effect of Discharge Voltage."*Vacuum Science and Technology* (1991), *A 9*, 124-127.

81. Alexander, P.M. and Hoffman, D.W. "Effects of Impurites on Intrinsic Stress in Thin Ni Films."*Journal of Vacuum Science and Technology* (1976), *13*, 96-98.

82. Pulk, H.K. "Mechanical Propetries of Optical Films."*Thin Solid Films* (1982), *89*, 191-204.

83. Machlin, E.S. *Materials Science in Microelectronics*; (Giro Press: Croton-on-Hudson, NY, 1995);